ABSTRACT

Modeling and Investigation of Current Transport Phenomena in Schottky Structures

by

Yan Zeng

We have used a numerical method to describe the importance of the contribution of generation-recombination current to the I-V characteristics of Schottky barrier contacts. The current-voltage relationship is derived directly from the fundamental set of equations such as Poisson; current-density and continuity equations, without having to make many simplifications or approximations. The final result includes not only the thermionic emission or drift diffusion mechanisms of current flow, but also the generation recombination processes.

The experimental devices used for this work are very common low barrier height Schottky structures, Al/$Ti_{0.3}W_{0.7}$/n-Si/Al and $Ti_{0.3}W_{0.7}$/n-Si/Al. The comparison between the measured and simulated results strongly showed the effect of recombination current as an important factor for even relatively low barrier height devices in the low bias region. From derived expression of the I-V characteristics, we can accurately fit the experimental results just simply by adding the term for the recombination effects. A good estimation for the values of recombination current effect can be calculated from I-V expression used for this work.

MODELING AND INVESTIGATION OF CURRENT TRANSPORT PHENOMENA IN SCHOTTKY STRUCTURES

by
Yan Zeng

A Thesis
Submitted to the Faculty of
New Jersey Institute of Technology
in Partial Fulfillment of the Requirements for the Degree of
Master of Science in Electrical Engineering

Department of Electrical and Computer Engineering

May 1993

APPROVAL PAGE

Modeling and Investigation of Current Transport Phenomena in Schottky Structures

Yan Zeng

5 10 93

Dr. N. M. Ravindra, Thesis Adviser (date)
Associate Professor of Physics, NJIT

5/10/93

Dr. D. Misra, Committee Member (date)
Assistant Professor of Electrical Engineering, NJIT

May 10, 93

Dr. Haim Grebel, Committee Member (date)
Associate Professor of Electrical Engineering, NJIT

BIOGRAPHICAL SKETCH

Author: Yan Zeng

Degree: Master of Science in Electrical Engineering

Date: May 1993

Date of Birth:

Place of Birth:

Undergraduate and Graduate Education:

- Master of Science in Electrical Engineering,
  New Jersey Institute of Technology, Newark, NJ, 1993

- Bachelor of Science in Electrical Engineering,
  Beijing University of Iron and Steel Industrial Technology,
  Beijing, P. R. China, 1982

Major: Electrical Engineering

To My Husband

ACKNOWLEDGMENT

I wish to express my sincere gratitude to my thesis advisor, Dr. N. M. Ravindra, for his advice, guidance, encouragement and friendship throughout my graduate work at New Jersey Institute of Technology as well as for his invaluable technical discussions, directions and help throughout the implementation, and preparation of this thesis.

I also wish to thank Dr. Madan Dubey of US Army Research Labs, Fr. Monmonth, for suppling the samples and helpful suggestions.

In particular, I would like to thank Dr. D. Misra and Dr. Haim Grebel for serving as members of the committee and careful reviewing of this thesis.

TABLE OF CONTENTS

LIST OF TABLES

Table **Page**

LIST OF FIGURES

CHAPTER 1

INTRODUCTION

The earliest systematic investigation on metal-semiconductor contacts goes back more than a hundred years to the work of Braun, who discovered the asymmetric nature of electrical conduction between metal contacts and semiconductors and noted the dependence of the total resistance on the polarity of the applied voltage and on the detailed surface conditions in 1874. Although the rectification mechanism was not clearly understood by that time, the point contacts between metal and metallic sulphides were extensively used as detectors in the early days of radio in 1904. In 1906, Pickard took out a patent for a point contact detector using silicon. In 1907, Pierce published rectification characteristics of diodes made by sputtering metals onto a variety of semiconductors.

It was one of the important early steps towards understanding the rectifying action of metal-semiconductor contacts, when Schottky and others showed that if a current flows, then the potential drop occurs almost entirely at the contact. In 1932, Wilson and others formulated the transport theory of semiconductors based on the band theory of solids. This theory was then applied to the metal-semiconductor contacts.

In 1938, Schottky and Mott independently pointed out that the observed direction of rectification could be explained by supposing that electrons passed over a potential barrier through the normal processes of drift and diffusion. Schottky suggested that the potential barrier could arise from a constant density of charged impurities so that the electric field increased linearly and the electrostatic potential quadratically, in accordance with Poisson's equation, as the metal was approached. The model arising from this consideration is known as the Schottky barrier. According to Mott, the potential barrier arose because of a difference between the work functions of the metal and semiconductor and he devised an appropriate theoretical model for swept-out metal-semiconductor contacts that is known as the Mott barrier.

In 1942, a significant advance which was considerably helped by developments in semiconductor physics came as an application of silicon and germanium point-contact rectifiers in microwave radar. Perhaps, the most important contribution during that time was Bethe's thermionic-emission theory which suggested that the current is determined by the process of emission of electrons into the metal, rather than by drift and diffusion in the semiconductor as was described by Mott and Schottky.

After 1945, stimulated by the fast development in the field of semiconductor physics which lead up to the invention of the point-contact device, the study on metal-semiconductor contacts eventually switched the attention towards extended-area contacts. Although point contacts used to be widely applied as detectors in the early days of radio and as microwave mixers and detectors later, they have now given way to the development of extended-area contacts because of the superior reproducibility and reliability of the latter.

During 1950s and 1960s, the important technology in metal-semiconductor fabrication consisted of evaporation of metal films in a conventional vacuum system. These films were much more stable and reproducible than point-contacts.

This technology was largely associated with the theoretical work of Bardeen, Crowell, and Sze, and the experimental work of Goodman, Archer, Atalla, and others. It laid the foundation for our present extensive knowledge of the subject.

During the past many years, the components based on Schottky barriers have been increasingly used in the area of solid state electronics. Research has continued with the object to approach a full understanding of the physics of barrier formation and the properties of current transport across metal-semiconductor interfaces. Since the early days of silicon technology, contacts between metal and silicon have presented a constant challenge to the electronics industry. There is a continuous demand for better contact metallurgy in order to tighten up the device design specifications. Many advanced techniques have been applied to probe the detailed microscopic interactions at the interfaces between metals and semiconductors. Theoretical methods have advanced in parallel, and computers have widely been applied to simulate the device fabrication processes and analyze the current transport phenomena.

CHAPTER 2

PHYSICAL PROPERTIES OF SCHOTTKY-BARRIER CONTACTS

2.1 Introduction

Because of their importance in the analysis of many fundamental physical properties, the metal-semiconductor contacts have been studied extensively. They are widely used as the gate electrodes of a field-effect transistor, the drain and source contacts on MOSFETs, electrodes for high-power IMPATT oscillators, the third terminal in a transferred-electron device, and photodetectors and solar cells. In this chapter, we will consider the general methods for formation of metal semiconductor contacts and the physical properties of the diffusion barrier by sputtering. The discussion will be mainly focused on the properties of $Ti_{0.3}W_{0.7}$/Si/Al and Al/$Ti_{0.3}W_{0.7}$/Si/Al structures which are very common structures and are the samples used for this work.

2.2 The General Formation of Metal-Semiconductor Contacts

Metal-semiconductor contacts can be formed by various methods. However there are two types of deposition processes that are very useful, chemical vapor deposition (CVD), and physical vapor deposition (PVD) namely evaporation and sputtering.

PVD is done under vacuum using either an evaporation or sputtering technique. In both cases, the formation of deposition on a substrate away form the source consists of three steps: (1) converting the condensed phase (generally a solid) into a gaseous or vapor phase, (2) transporting the gaseous phase from the source to the substrate, and (3) condensing the gaseous source on the substrate, followed by the nucleation and growth of the film. Although evaporation and sputtering processes are physically very different, certain behavior of the species in the gas phase are governed by the same principles.

Physical vapor deposition (PVD) by sputtering is quite extensive. Sputtering is a physical phenomenon used to describe the mechanism in which atoms are dislodged from the surface of a material by collision with high energy particles. It has become the most widely utilized deposition technique for a variety of metallic films in VLSI fabrication, including aluminum, aluminum alloys, platinum, gold, titanium:tungsten and tungsten. Through a potential gradient and the bombardment by the accelerated ions of a target or cathode and momentum transfer, atoms near the surface of the target material become volatile and are transported as a vapor to the substrate. It is desirable that as many of these sputtered atoms as possible be deposited upon the substrate and form the specified thin film through deposition. Sputtering process, unlike evaporation, is very well controlled and is generally applicable to all materials. The methods of radio frequency, dc and dc-magnetron sputtering can be used for metal deposition. Alloy-film deposition by sputtering from an alloy target is possible because the composition of the film is locked to the composition of the target. Alloys can also be deposited with excellent control of composition by using the individual component targets. Sputtering has replaced evaporation as the workhorse PVD method for VLSI because of its many advantages.

Deposition of films by thermal evaporation is the simplest method but is not as extensively used as sputtering in VLSI applications. Most evaporated contacts are made in a conventional vacuum system. The film is deposited by the condensation of the vapor on a substrate, which is maintained at a lower temperature than that of the vapor. All metals vaporize when heated to sufficiently high temperatures. Several methods, such as resistive, inductive, electron bombardment or laser heating can be used to attain these temperatures. The lower-melting-point metals such as aluminum and gold can usually be evaporated quite simply by resistive heating from a boat or filament, while the refractory metals like molybdenum and titanium are generally evaporated by electron-beam heating. The evaporation method can also be used to deposit an alloy or a mixture of two or more materials by using two or more independently controlled evaporation sources.

Chemical vapor deposition (CVD) for metal deposition in integrated circuit production has been one of the important applications in the area of refractory-metal deposition. CVD is attractive for metallization because it offers several advantages of which three are very important: (1) excellent step coverage, (2) large throughput, and (3) low-temperature processing. Tungsten and molybdenum which are common metals for forming the metal-semiconductor contacts have been very successfully deposited using LPCVD (low-pressure chemical vapor deposition). The following two chemical reactions show examples of CVD processing for both pyrolysis and the reduction of tungsten:

$$WF_6 \longrightarrow W + 3F_2$$

$$WF_6 + 3H_2 \longrightarrow W + 6HF.$$

CVD tungsten has been investigated for a variety of applications in both metal-Si contacts and interconnect structures.

2.3 The Properties of Diffusion Barrier Ti-W

After having briefly reviewed the general fabrication methods for metal-semiconductor contact formation, let us begin to look at the properties of Al/Si, and $Al(1\%Si)/Ti_x\text{-}W_{1-x}/Si/Al(1\%Si)$ structures. Aluminum has been used traditionally as interconnect and contact material in integrated circuits. The contact structure consisting of pure Al deposited directly onto Si was adopted in the earliest stages of silicon technology primarily because of its simplicity and other advantages. Al and Al-alloy are still widely used for metallization in IC processes today. However, the Al-to-Si contact exhibits some poor contact characteristics and also introduces some limitations into the processing sequence.

Apart from its desirable properties such as low resistivity (i.e., $2.7\mu\Omega$-cm for Al and up to $3.5\mu\Omega$-cm for its alloys), good adherence, and plasma etching behavior, aluminum suffers from its tendency to interact with silicon, silicides, gold, and other materials used in interconnection schemes. The melting point of pure aluminum and pure silicon are 660 and 1412°C, respectively. Because of the eutectic characteristics, during aluminum deposition, the temperature on the silicon substrate must be limited to less than 577°C. Fig. 1 [16] presents the solid solubility of silicon in aluminum. After aluminum has been deposited and delineated on the silicon substrate, it is common practice to carry out a post-aluminum-metallization anneal at around 400°C or higher to reduce the concentration of metal defects. Hence, wherever aluminum contacts silicon, the silicon will dissolve into the aluminum during annealing. The amount of silicon removed from the contact depends on the amount of aluminum coverage on top of the silicon contact and the annealing temperature and time. Possibly as a result of the non-uniformity of the silicon native oxide and the asymmetry of the top aluminum pattern, the depletion of silicon in a contact hole is highly non-uniform. Spiking is a major problem which will cause the device failure. For instance, when the aluminum spikes penetrate the *p-n* junction, the junction will exhibit large leakage currents or even become electrically shorted.

Silicon pits and aluminum spikes are usually formed at localized spots, particularly along the periphery of the contact opening. One way to minimize the aluminum spiking without abandoning the advantages of the simple Al-to-Si contact structure is by simply adding 1% ~ 2% Si to the aluminum to presaturate the aluminum. Although this simple solution of 1% ~ 2% Si in Al instead of pure Al is effective in preventing spiking, it also leads to other problems. During the cooling cycle of a thermal anneal, the solid solubility of silicon in aluminum decreases with decreasing temperature. The aluminum thus becomes supersaturated with Si, which causes nucleation and growth of Si precipitates out of the Al:Si solution. For smaller contacts, the situation will be aggravated. When we talk about scaled-down devices which means the device becomes smaller, the corresponding current density becomes larger. As high current densities are passing through Al-Si contacts, the electron current leads to the transport of Si from the contacts into the Al. This causes the spiking at the negative terminal and deposition of Si at the positive terminal that causes the device failure due to the phenomenon of electromigration. As a result, more elaborate contact structures have to be developed in order to overcome those limitations of the simple Al (1% ~ 2%Si) structures.

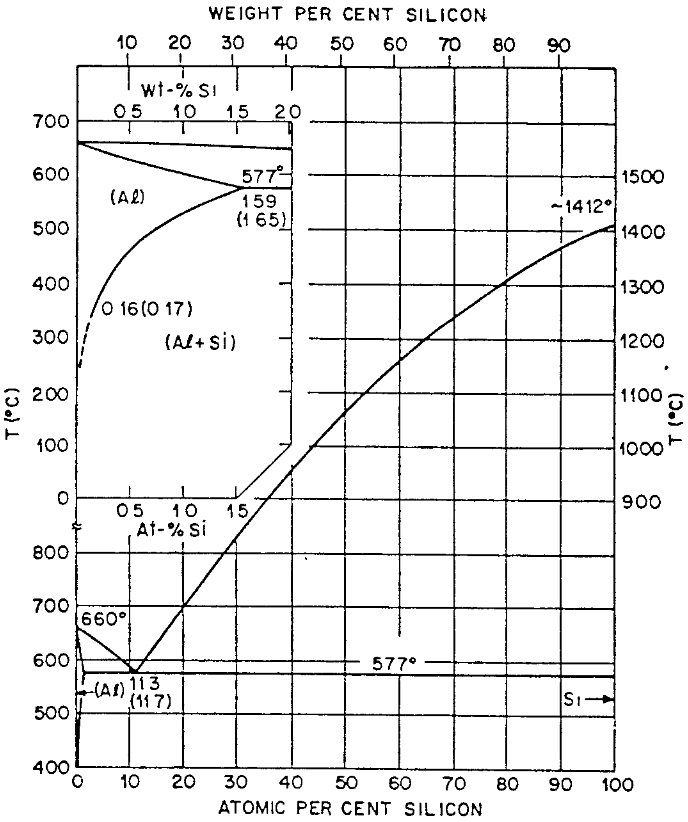

Fig. 1 Phase diagram of aluminum-silicon system. [16]

One of the effective methods is to introduce a barrier metal layer between the aluminum and the silicon substrate. Typically a PtSi layer, created by reacting a thin Pt film with the Si substrate, forms a predictable, albeit high barrier Schottky contact to the Si. Because the PtSi-Si contact structure exhibits some limitations, further improvements have to be introduced.

The intermixing of materials from two layers in contact can be prevented by sandwiching another material between them. The role of this third material is to prevent the diffusion of the two original materials into each other, or to resist the tendency of a chemical reaction to form a new phase between the adjoining materials. Many of the various materials have been suggested as diffusion barriers in the integrated circuit fabrication. The one that has been most widely adopted is the structure $Ti_{1-x}W_x$. The Ti-W metallization system was first proposed [10] for integrated circuit application to improve the thermal stability and corrosion resistance of contacts with gold wire bonding and plastic packaging. Since then, a great deal of work [19, 11, 21, 15] has been done on the physical and electrical properties of the Ti-W contact system. Nowicki et al. and Hill [21, 17] reported respectively that $Ti_{0.3}W_{0.7}$ acts only as a marginal diffusion barrier when deposited in a relatively pure state and as an effective diffusion barrier between aluminum and gold when deposited in a relatively impure state, such as by sputter deposition in a mixed N_2-Ar ambient.

Sputter deposited titanium-tungsten which is usually named stuffed barrier was among the earliest materials to be used as a diffusion barrier. While tungsten is by itself a fairly good diffusion barrier, because the contacts made with W as the barrier layer can withstand temperature of up to 450°C [27], the Ti is added for several reasons. First, tungsten does not adhere well to "clean" Si, Ti can improve this adhesion problem of the W to SiO_2. Secondly, it protects the tungsten from corrosion by forming a thin layer of titanium oxide on the surface, making the tungsten an even better diffusion barrier. Finally, the maximum temperature that the alloy contacts can withstand is increased to ~500°C [27]. For major practical fabrication, Ti-W films are normally sputtered from a single target or cathode composed of $Ti_{0.3}$ $W_{0.7}$ (10:90 wt%). The films deposited from such targets show resistivities of 60 ~100 $\mu\Omega$-cm depending on the deposition conditions. Deposition may be accomplished using rf diode or dc and rf magnetron sputtering systems. The resistivities of the pure TiW layers agree very well with the data reported elsewhere for dc magnetron sputtered films. In the contact metallization system, the TiW barrier will not act as an absolute barrier. During annealing the following reaction will occur:

$$Ti + 3Al \longrightarrow TiAl_3\ (400°C)$$
$$W + 12Al \longrightarrow WAl_{12}\ (450 \sim 500°C)$$

This is an unexpected interdiffusion process which will destroy the contact structure.

The reactions between Ti or W and Si are relatively slow compared to those with Al. As long as some unreacted barrier metal remains, the contact retains its structural integrity. This is an important factor for extending the lifetime of the barrier layer. The process of sputter deposited TiW is normally carried out in an Ar-N_2 ambient, so that nitrogen may become an impurity in the TiW film [20]. It is believed to have two effects for this situation, first, it may "stuff" the grain boundaries and thereby substantially reduce the rate of interdiffusion; secondly, it may decrease the reactivity, especially of Ti, by TiN formation and thereby enforce the chemical stability of the barrier layer. Both the effects will increase the lifetime of the barrier layer.

When the TiW layer is totally consumed, two other reactions may happen: dissolution of Si into the Al to cause spiking and formation of Si compound with $TiAl_3$ and WAl_{12} and the barrier characteristic may no longer exist. A reduction of degradation phenomenon has been found with a few monolayers of oxygen at the Al/TiW interface. This is practiced by using two separate deposition systems for TiW and Al(1%Si). Now, there is a tendency to perform both the TiW and Al deposition in one system which can further improve the barrier for contact metallization to achieve the high reliability barrier performance. The use of TiW structure for the diffusion barrier, also has some sorts of drawback for VLSI and ULSI processing. The TiW film is quite brittle and highly stressed upon being deposited.

CHAPTER 3

ELECTRICAL PROPERTIES OF SCHOTTKY BARRIER CONTACTS

When a metal is making contact with a semiconductor, a barrier will be formed at the metal-semiconductor interface. In this chapter, we will briefly consider the basic energy band diagrams based on Schottky-Mott model, the depletion layer of Schottky contact and the image force effect. The major discussion will be focused on the important parameter of the barrier heights for Ti-W/Si and Al/Ti-W/Si/Al structures. The current transport properties will be the topic in the next chapter.

3.1 The Basic Energy Band Diagrams for Schottky Barrier

It is convenient for discussion to introduce the surface parameters which are the work function ϕ of a solid and the electron affinity χ of semiconductor. The work function is the energy difference between the Fermi energy and the ionization energy and the electron affinity is measured from the bottom of the conduction band to the vacuum level. Typical values of ϕ for very clean surfaces are 4.28, 4.33 and 4.55eV for Al, Ti and W respectively [7]. These values may have different values due to surface dipoles of unequal magnitudes and other related reasons.

When a metal comes into contact with a semiconductor, the Fermi levels in the two materials must be continuous at thermal equilibrium. Here, suppose that the metal and semiconductor are both electrically neutral and separated from each other, the contact between them is in the absence of surface states.

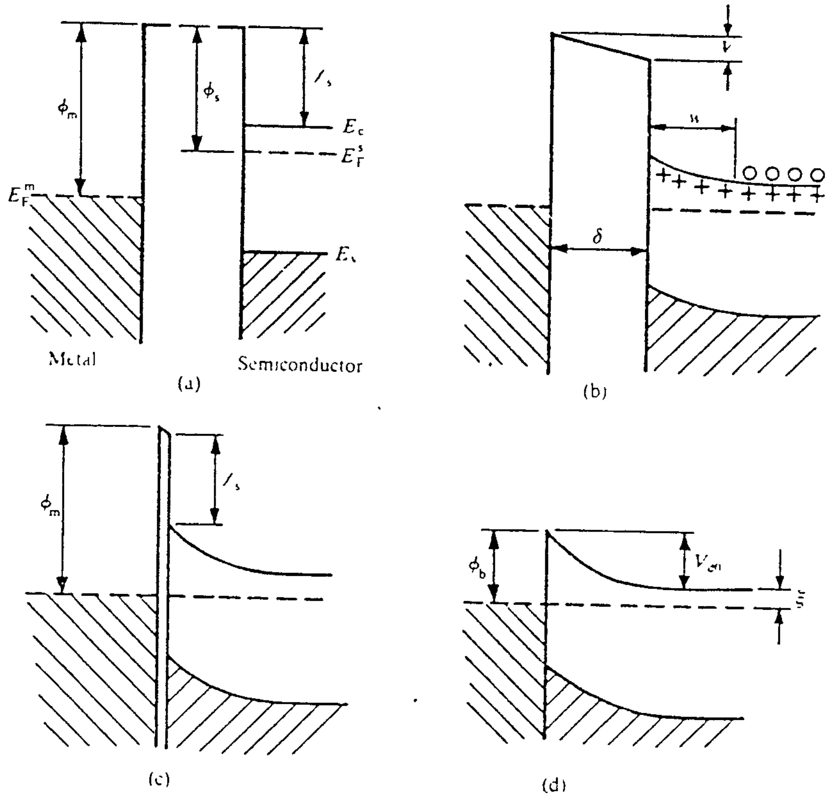

Fig. 2 Formation of a barrier between a metal and a semiconductor (a) neutral and isolated, (b) electrically connected, (c) separated by a narrow gap, (d) in perfect contact. o denotes electron in conduction band; + denotes donor ion[7].

In practice the most important case is that of an n-type semiconductor with a work function less than the metal. The corresponding energy band diagram is shown in Fig. 2(a). If a wire is connected between a metal and semiconductor so that the electrons will pass from semiconductor to the metal, the two Fermi levels are forced into continuity and band bending upwards occurs as is shown in Fig. 2(b). When the difference Vi between the electrostatic potential and the semiconductor tends to zero, the ideal situation will look like Fig. 2(c) and Fig. 2(d). This energy band diagram only shows the ideal case. A more general situation should include the effects of surface states, the interfacial layer and the image force which will be detailed in the next section.

3.2 The Depletion Region, Image Force Effect and Barrier Height

When a metal is brought in contact with a semiconductor, charge transfer occurs until the Fermi levels align at equilibrium. To align the two Fermi levels, the electrostatic potential of the semiconductor must be raised relative to that of the metal. In the n-type semiconductor, a depletion region W is formed near the junction. The positive charge due to uncompensated donor ions within W matches the negative charge on the metal. The electric field and the bending of the bands within W are similar to the effects of the one-sided abrupt p^+-n junctions.

Assuming that there is no interfacial layer existing between a metal and semiconductor, when an electron approaches a metal, the requirement that the electric field must be perpendicular to the surface enables the electric field to be considered as if there were a positive charge located at the mirror-image of the electron with respect to the surface of the metal. When this sort of image force is combined with an applied electric field, the effective metal work function is somewhat reduced. This phenomenon has been described as Schottky effect which is the image force induced lowering of the potential energy for charge carrier emission when an electrical field is applied. The image potential energy has to be added to the potential energy due to the Schottky barrier. If there is an insulating layer between the metal and the semiconductor, the potential due to the image force will be much more complicated. Because the image force lowering contributes to modification to the barrier height of the Schottky structure, even in a perfect contact without interfacial layer, the barrier height is still reduced as a result of the image force by an amount $\Delta\phi$.

The barrier height is the most important parameter to describe the behavior of the Schottky barrier contacts. Specifically, an investigation of the thermal stability and Schottky behavior of sputter deposited $Ti_{03}W_{07}$ diffusion barrier contact to n-Si in the presence of an Al overlayer is reported by Babcock et al. [23] In previous experiments [24], the structure of $Ti_{03}W_{07}$ thin film contact to n-Si was found to form a low Schottky barrier height of 0.51 ~ 0.55eV and was stable up to 30 min. anneals at 550°C. This contact is quite unique for another reason i.e., repeatable Schottky contact behavior was obtained without silicide formation. For the low barrier height structures of $Ti_{03}W_{07}$/n-Si/Al(1%Si) and Al(1%Si)/$Ti_{03}W_{07}$/n-Si/Al(1%Si), the barrier height and current transport properties will be discussed further in the next chapter.

3.3 Surface Effects and Recombination-Generation Phenomena on Metal- Semiconductor Contacts

The barrier heights and the current-voltage characteristics are two of the most important areas of investigation of metal-semiconductor contacts. The properties of the barrier height have been presented briefly in section 3.2 and will be discussed further in the next chapter.

The surface effects are indeed of great importance in determining the I-V characteristics of metal-semiconductor contacts because the current-voltage characteristics of metal-semiconductor contacts usually deviate from the ideal behavior. Many of the non-ideal characteristics of metal-semiconductor contacts can be understood in terms of the properties of the space-charge region at the edge of the contacts.

We have considered the basic band diagrams of metal-semiconductor contacts in section 3.1. The Schottky-Mott model, described in 3.1, is based on the Schottky-Mott theory. which is an ideal case. In most practical metal-semiconductor contacts, the ideal situation is never reached because there is usually a thin insulating layer of oxide on the surface of the semiconductor. Such an insulating film is often referred to as an interfacial layer. The Bardeen model [41] represents a good insight into the general features of interface state behavior. It supposes that there are localized states at the insulator-semiconductor interface and has the merits of being easy to analyze and of corresponding to the real cases of the metal-semiconductor contacts. A detailed energy-band diagram of a metal n-type semiconductor contact is therefore more like that shown in Fig. 3 [25].

In the presence of surface states, the neutrality condition becomes $Q_M = -(Q_{SS} + Q_{sc})$. There are three distinct sources of charge in the system: Q_M resides on the surface of the metal, Q_{sc} is due to the uncompensated donor ions in the depletion region and Q_{SS} is due to electrons in the surface states. Q_M is determined by the electric-field strength in the insulating layer, Q_{sc} by the width of the depletion region and the density of donors, and Q_{SS} is determined by the density of interface states and by their occupation probability. These three charge desities are the important factors describing the phenomena of surface effects.

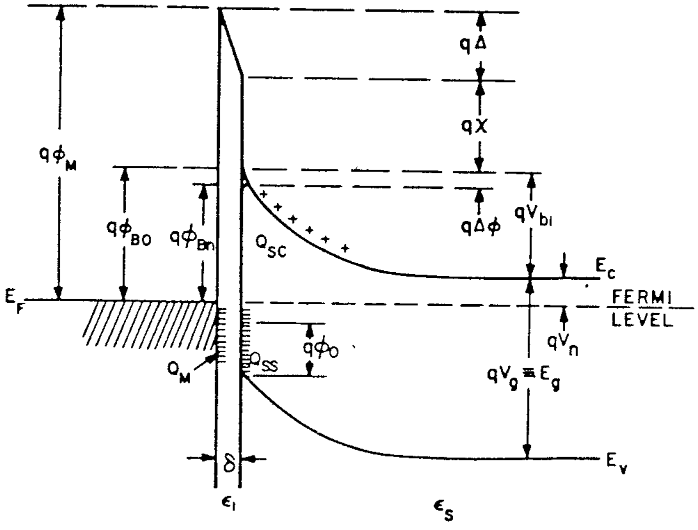

Fig.3 detailed energy band diagram of a metal n-type semiconductor contact with an interfacial layer of the order of atomic distance (all symbols have their usual meaning) [25].

The depletion regions and the corresponding energy-band diagrams are different for various bias conditions. The flat-band voltage can be considered as a voltage just sufficient to overcome the "built-in" voltage due to the metal-semiconductor work-function difference and surface state charge Q_{ss}. The energy band comes up flat to the surface and the potential barrier at the edge of the metal contact looks the same going along the surface. When a bias more negative than the flat-band voltage is applied, a surface depletion layer is formed. It is continuous with the depletion layer of the metal-semiconductor contact. If a bias further more negative than the flat-voltage is applied, the surface depletion region is widened and a layer of strong inversion is formed. If a bias more positive than flat-band voltage is applied, the energy band is bent down at the surface, forming an accumulation layer and causing the potential barrier of the metal-semiconductor contact to be narrower in the direction along the surface. The forward as well as the reverse I-V characteristics of an metal-semiconductor contacts can be substantially modified by varying the applied voltage and consequently the condition of the space-charge region where it intersects the surface.

In earlier studies about Schottky barrier contacts have represented the experimental results of the current components in metal-semiconductor contacts. The phenomena and importance of recombination in the space charge region have been demonstrated by Yu and Snow [2]. They showed that both the forward and reverse currents of a metal-semiconductor contact increase to a higher level when the surface around the contact is inverted. This increase is due to generation-recombination currents associated with the field-induced junction. When the positive bias is applied and the surface is accumulated, excess current will appear. The forward excess current will be relatively less important as the forward bias is increased. The surface may be accumulated by the positive interface charge Q_{ss} or by positive ions in the oxide or on the oxide surface. Therefore, depending on the surface condition, a given metal-semiconductor contact may have widely different I-V characteristics. The surface condition is determined by the amount of charge on or near the surface. Because of the presence of positive surface state charge at the interface and positive ions in or on the oxide, the surface of n-type Si is usually accumulated. The mechanism such as recombination current in the depletion region can be well understood after considering the phenomena of surface effects on metal-semiconductor contacts.

CHAPTER 4

MODELING AND EXPERIMENTAL STUDIES OF CURRENT TRANSPORT THROUGH THE SCHOTTKY STRUCTURE

4.1 Introduction

In this study, it is attempted to interpret the experimentally observed and theoretically numerically described non-ideal Schottky-barrier I-V characteristics considering the effects of generation-recombination processes in the analyzed structure. The transport of electrons over the potential barrier will be considered. For high-mobility semiconductors such as Si, the transport could be adequately described by the thermionic emission theory. The diffusion theory and the generalized thermionic-diffusion theory which is the synthesis of the preceding two theories will also be considered. By introducing a more general and theoretical treatment of the current transport process, besides the thermionic-emission or drift-diffusion mechanisms of current flow, the generation recombination current will be taken into account.

4.2 Current Transport Theory

In this section, we begin to discuss the transport mechanisms that determine the conduction properties of Schottky barriers. Here it is assumed that a barrier has been established and assume nothing about the factors which determine the height of this barrier. Because of their importance in direct current and microwave applications and as tools in the analysis of important fundamental physical parameters such as the magnitude of the barrier heights, metal-semiconductor contacts and the processes of current transport through the contacts have been studied extensively. The current transport in metal-semiconductor contacts is mainly due to majority carriers. Many theories that describe various mechanisms of the current transport across the metal-semiconductor interface have been developed. The various ways in which electrons can be transported across a metal-semiconductor junction under forward bias are shown schematically for a n-type semiconductor (in this work, we only discuss the n-type silicon) in Fig. 3 [25] The inverse processes occur under reverse bias. The four mechanisms are:

(1) emission of electrons from the semiconductor passed up the top of the barrier into the metal (this process is dominant for Schottky contacts with moderately doped semiconductors and operated at 300 K);

(2) quantum-mechanical tunneling through the barrier, it is important for heavily doped semiconductors and most ohmic contacts;

(3) recombination process in the space-charge region;

(4) recombination process in the neutral region ('hole injection' from the metal to the semiconductor).

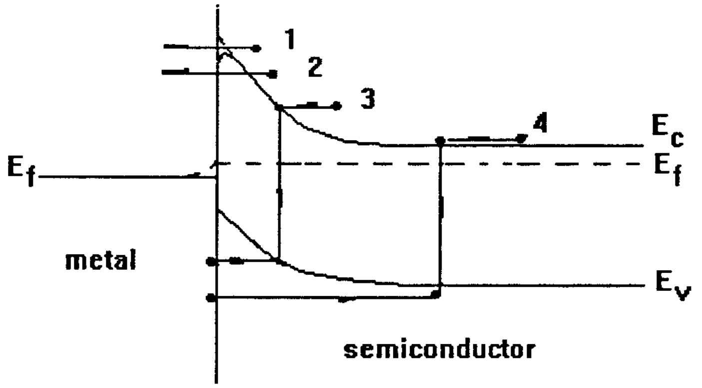

Fig.4 Four basic transport processes under forward bias [25].

The main question is to solve these problems whether the current is limited by the process of thermionic emission of electrons from the semiconductor into the metal, as was considered by Bethe (1942), or whether it is limited by drift and diffusion of electrons through the space charge region, as was suggested in the original works of Schottky and Spenke (1939) or Mott (1938). It is possible to make practical Schottky-barrier contacts in which process (1) were the most important and such contacts are generally referred to as "nearly ideal". The I-V characteristics of metal-semiconductor diodes are often termed "ideal" if they can be described in the process of the thermionic emission of conduction electrons over the interfacial potential barrier alone. Processes (2), (3), and (4) usually are the important factors causing departures from the so called ideal behavior. In traversing the depletion region of the semiconductor, the motion of electrons is governed by the usual mechanism of drift and diffusion in the electric field of the barrier. According to the diffusion theory of Schottky and Spenke, such diffusion process is the major limiting factor. The diffusion theory of Schottky is derived by using current density equation and is expressed as:

$$J_n \cong \{\frac{q^2 D_n N_c}{kT}[\frac{q(V_{bi} - V)2N_D}{\varepsilon_s}]^{1/2} \exp(-\frac{q\phi_{Bn}}{kT})\}[\exp(\frac{qV}{kT}) - 1]$$

$$= J_{SD}[\exp(\frac{qV}{kT}) - 1] \qquad (1)$$

where J_{SD} is saturation current density due to diffusion.

When electrons arrive at the interface, their emission into the metal is determined by the rate of transfer of electrons across the boundary between the metal and the semiconductor, whereas according to the thermionic-emission theory of Bethe the thermionic-emission process is more important. In Bethe's thermionic-emission theory, the assumption is made that the current-limiting process is the actual transfer of electrons across the interface between the semiconductor and the metal. The total electron current density is given by:

$$J_n = [A^{**}T^2 \exp(-\frac{q\phi_{Bn}}{kT})][\exp(\frac{qV}{kT}) - 1] = J_{ST}[\exp(\frac{qV}{kT}) - 1] \qquad (2)$$

where J_{ST} is saturation current density due to thermionic emission.

These two processes that are described by the expressions (1) and (2) are effectively in series, and the current is determined pre-dominantly by whichever causes the larger impediment to the flow of electrons. The two expressions of the drift-diffusion and thermionic-emission theories in equations (1) and (2), are basically very similar. They are almost of the form of the ideal rectifier characteristic $J = J_0[\exp(qV / kT) - 1]$. The difference arises because the saturation current density of diffusion theory J_{SD} varies more rapidly with the bias voltage. In fact, the current does not saturate but increases roughly as $|V|^{1/2}$ for large values of reverse bias. However, J_{SD} is less sensitive to temperature compared with J_{ST}. A more accurate difference between the two theories is well brought out by the behavior of the quasi-Fermi level for electrons in the conduction band of the semiconductor.

By considering both the mechanisms to be in series and effectively finding the position of the quasi-Fermi level at the interface the synthesis of the thermionic emission and drift diffusion theory has been described by several authors [29, 3, 5]. The most complete combined theory of transport process in metal-semiconductor systems was developed by Crowell and Sze [5] who introduced the concept of "recombination velocity" v_R at the top of the Schottky barrier. Their approach was derived from the boundary condition of a thermionic recombination velocity v_R near the metal-semiconductor interface. From their derivation the final formula for electron current density can be expressed in the form:

$$J = \frac{qN_c v_R}{1 + v_R / v_D} \exp\left(-\frac{q\phi_{Bn}}{kT}\right)\left[\exp\left(\frac{qV}{kT}\right) - 1\right] \tag{3}$$

where

$$v_D \equiv \left\{ \int_{x_m}^{w} \frac{q}{\mu_n kT} \exp\left[-\frac{q}{kT}(\phi_{Bn} - \psi)\right] dx \right\}^{-1} \tag{4}$$

is an effective diffusion velocity associated with the transport of electrons from the edge of the depletion region to the potential energy maximum, $v_R = A_n^{**}T^2/qN_c$, is the electron recombination velocity, A_n^{**} is the modified Richardson constant, ϕ_{Bn}

is the barrier height and $q\psi(x)$ is the electron potential energy within the analyzed structure.

The significance of ν_D is that the term $\{\nu_D\, [\exp(qV / kT) - 1]\}$ represents the mean velocity due to drift and diffusion of electrons at the top of the contact barrier if $\nu_D << \nu_R$, the diffusion theory were to apply. If $\nu_D >> \nu_R$, the pre-exponential term in Eq. (3) is dominated by ν_R, and the current flow is the actual emission of electrons into the metal so that the thermionic emission theory most nearly applies. The concept of a recombination velocity is quite general and can be applied effectively. Before discussing other concepts of current transport processes, the effect of the image force between an electron and the surface of the metal must be taken into account. When considering the I-V characteristics under the condition of thermionic emission, the ideal rectifier I-V characteristics are given by

$$J = J_0\, [\exp(qV / kT) - 1],$$

where $J_0 = A^{**}T^2 \exp(-q\phi_B / kT)$, with the barrier height being considered as independent of bias. However, this is not so accurate. In a real device, the barrier height always depends on the electric field in the depletion region and hence on the applied bias. [7]. Particularly, even in a perfect contact with no interfacial layer, because of the effect of image-force, the barrier height is still reduced by an amount $\Delta\phi$ which depends on the bias voltage. The effective barrier that electrons must surmount before they can reach the metal can therefore be written as

$$\phi_{Bn}(V) = \phi_{B0} - \Delta\phi(V). \qquad (5)$$

The effect of the image force lowering can easily be considered if the voltage dependence of the barrier height is linear. To include this effect on the calculation of v_D, the appropriate expression for $\psi(x)$ in Eq. (4) is

$$\psi(x)= \phi_{Bn} + \Delta\phi - Ex - \frac{q}{16\pi\varepsilon_s x} \qquad (6)$$

where E is the field strength and $\Delta\phi$ is the barrier lowering as given by the equation:

$$\Delta\phi = \sqrt{\frac{qE}{4\pi\varepsilon_s}}. \qquad (7)$$

Such a bias dependence of effective barrier height could modify the I-V characteristic and it always increases with increasing forward bias. For considering this effect, we note that the current density expression of thermionic-emission theory discussed before can be written in the form

$$J = J_0 \exp(qV / nkT) [1 - \exp(- qV / kT)] \qquad (2a)$$

Where *n* is the 'ideality factor' which is an important parameter for Schottky diode and can be obtained from the experimental I-V characteristics. The value of *n* is usually very close to unity at low doping and high temperature. However, it can depart substantially from unity when the doping is increased or the temperature is lowered. As we shall see shortly in the next section, there are other mechanisms besides a bias dependence of the effective barrier height, notably the recombination process in the depletion region, which yield relationship similar to Eq. (2a).

As mentioned before, mechanisms (2) (3) and (4) may lead to difference between theoretical and experimental characteristics. To explain these discrepancies, theories describing different mechanisms of current flow were developed. Under certain circumstances, it may be possible for electrons with energy below the top of the barrier to penetrate the barrier by quantum-mechanical tunneling. In the case of heavily doped semiconductor or for operation at low temperature, the tunneling current may become the dominant transport process. The extension of the theory of tunneling through Schottky barriers beyond a simple analysis is mathematically very complicated and has been developed by Padovani and Stratton [8] and by Crowell and Rideout [28]. The Schottky barrier formed on most semiconductors produces diodes which are essentially majority-carrier devices under low injection conditions. In view of this, Schottky structures have been analyzed largely as single carrier systems. The contribution of minority carrier injection was analyzed by Scharfetter [6] who has shown that minority carriers can affect the diode properties under moderate to large forward bias conditions. If the barrier height on n-type material is greater than half of the band gap, as it is often the case, the region of the semiconductor adjacent to the metal becomes p-type and contains a high density of holes. At sufficiently large forward bias, one might expect some of these holes to diffuse into the neutral region of the semiconductor and the minority-carrier injection ratio increases with current due to the enhancement of the drift-field component. Hole injection at metal contacts was extensively studied in the early days of semiconductors, and the previous works have been summarized by Henisch [9]. A more important effect of generation-recombination current is the other common cause of departure from ideal behavior in Schottky structures. This will be the major topic of discussion in the following sections. As shown above, all the mentioned theories lead, more or less, to final expressions where the current density is expressed as an analytical function of the applied voltage. They are applied under some reasonable simplifications to satisfy many simple and convenient numerical calculations. In sections 4.3 and 4.4, the numerical calculation and analysis of the effect of generation-recombination process for current transport across the Schottky contacts and the experimental I-V method of measurement of barrier heights are presented. The thermionic-emission/ drift-diffusion mechanisms of current transport and the generation-recombination processes have been considered for this analysis. The comparison between calculated I-V characteristics and experimentally measured results on the Schottky structures of $Ti_{03}W_{07}$/n-Si/Al and Al/$Ti_{03}W_{07}$/n-Si/Al have been presented.

4.3 Calculations of the Effects of Generation-Recombination Processes

The importance associated with the influence of the generation and recombination current in the space-charge region was first convincingly considered in a classic paper by Yu and Snow [2]. Recently, the further study has been developed by Racko et al. [13] In their work, Racko et al. have presented a new treatment of the theory describing the carrier transport across the rectifying metal-semiconductor interface. By including the thermionic emission/drift-diffusion current, generation-recombination current and injection of holes into the quasi-neutral semiconductor region, they derived a general solution that is a more theoretical formulation but still may not be directly useful for numerical analysis. It is the purpose of this thesis to present an improved analytical and a realistic expression based on

Racko's approach for the numerical analysis of the practical problems, and to get the results for a particular structure $Ti_{0.3}W_{0.7}$/n-Si/Al and Al/$Ti_{0.3}W_{0.7}$/n-Si/Al. The expressions for the current-voltage relations are obtained through a direct derivation from the basic equations and convenient choices of unknowns. A comparison with experimental results will be presented in the following section.

Considerable attention is focused on the numerical analysis of the problem to explain the experimental phenomena. In order to achieve analytical results, a number of assumptions in the model and approximations in the set of equations have to be consistently introduced; several 'first-order' results, valid in certain ranges of the relevant quantities and for a limited number of specialized structures, have to be given.

In many moderately doped Schottky structures, more important contribution to the current voltage characteristics, apart from that ideal situation due to thermionic emission, is the contribution that arises from the recombination of electrons in localized states in the depletion region. And according to the theory considered in detail by Shockley and Read [29], Hall [30], the most effective centers are those with energies lying near the center of the forbidden gap of the semiconductor. The theory of current conduction due to such recombination centers in Schottky structures is quite similar to that for p^+- n junctions. The analysis discussed in this paper is restricted to the steady-state condition. The following assumptions are introduced:

(1) time-independent impurity distribution
(2) moderately doped semiconductors (Si with $N_D \leq 10^{17}$ cm^{-3})
(3) constant temperature (300 K)
(4) full ionization of the impurities

(5) non-degenerate conditions (for validity of the Boltzmann statistics).

The discussion is restricted to uniformly and moderately doped devices of planar geometry with a Schottky barrier contact to the semiconductor and an ohmic back contact. The back contact is modeled as an ideal ohmic contact i.e., at the contact, space charge neutrality and thermal equilibrium are assumed. The equations describing carrier behavior within the semiconductor are the group of familiar basic equations of semiconductor device physics, i.e., the Poisson's equation, the current density equations and the electron and hole continuity equations.

$$\nabla E = \frac{q}{\varepsilon}(p - n + N_d - N_a) \tag{8}$$

$$J_n = q\,\mu_n\, n\, E + q\, D_n\, \nabla n \tag{9}$$

$$J_p = q\,\mu_p\, p\, E + q\, D_p\, \nabla p \tag{10}$$

$$\frac{\partial n}{\partial t} = G_n - R_n + \frac{1}{q}\nabla \bullet J_n \tag{11}$$

$$\frac{\partial p}{\partial t} = G_p - R_p - \frac{1}{q}\nabla \bullet J_p \tag{12}$$

where the symbols have their usual meanings [25], and for non-degenerate semiconductors the carrier diffusion constants (D_n and D_p) and the mobility are given by the Einstein relationship:

$$D = \mu \frac{kT}{q} \tag{13}$$

If we regard the position of the quasi-Fermi level $\zeta(0)$ at the interface, where the barrier height reaches its maximum value, and the image force is taken into account, the quasi-Fermi level $\zeta(x_m)$ at the maximum of the barrier should be used rather than $\zeta(0)$. Due to barrier height lowering, the interface lies inside the semiconductor but the displacement from the real surface is very small. It could be neglected by setting $x_m = 0$ for the purposes of convenience, but the lower limit of the integration will be x_m instead 0 using for calculations. Since the thermionic-emission current $J_{thn}(0)$ must equal the current $J_{dn}(0)$ determined by drift-diffusion i.e., $J_n(0) = J_{thn}(0) = J_{dn}(0)$ on the top of the interface of the semiconductor, $\zeta(0)$ could be eliminated between them through derivations procedure [7]. The majority carrier current flow across the contact is given by

$$J_n(0) = J_{thn}(0) = J_{dn}(0) = q\, v_R \,(n_s(0) - n_0). \qquad (14)$$

where $n_s(0)$ is the actual surface concentration of electrons, n_0 is the concentration which would occur if the electron concentration at the surface were computed using the metal Fermi-level. n_0 is defined as:

$$n_n = N_C \exp(-\frac{q\phi_{Bn}}{kT}) = N_C \exp(-\frac{\phi_{Bn}}{V_t}) \qquad (15)$$

where ϕ_{Bn} is the effective barrier height. The actual value of ϕ_{Bn} will be introduced for calculations of the I-V characteristics by referring to the measurement results. The calculated results will be compared with the experimentally measured I-V characteristics in section 4.4, The barrier height lowering $\Delta\phi$ introduced in section 4.2 is given by [25, 7]:

$$\Delta\phi = \{\frac{q^3N}{8\pi^2\varepsilon_s^3}[\phi_{Bn} + \Delta\phi - V - V_t(\ln\frac{N_C}{N_D} + 1)]\}^{1/4} = \sqrt{\frac{qE}{4\pi\varepsilon_s}} \tag{16}$$

The range of calculated values of barrier height lowering $\Delta\phi$ is given by:[40]

$$\Delta\phi = (\frac{qE_m}{4\pi\varepsilon_s})^{1/2} + \alpha E_m \tag{17}$$

where the first term is caused by the image force and the second term is due to the penetration of the electron wave function from metal to semiconductor. α is a constant and has value of 1.15 nm [14]. E_m is the maximum field strength which is expressed as:[25]

$$E_m = \{\frac{2qN_D}{\varepsilon_s}[\phi_{Bn} - V - V_t(\ln\frac{N_C}{N_D} + 1)]\}^{1/2} \tag{18}$$

v_R is the effective recombination velocity and if the effects of optical-phonon scattering and quantum-mechanical reflections in the contact region are included, its value is reduced but remains essentially bias independent at least for silicon. v_R is taken as constant and is defined as [26]:

$$v_R = \frac{A_n^{**}T^2}{qN_C} = 2.2 \times 10^6 \text{ cm/s} \tag{19}$$

where $A_n^{**} = 110$ A/cm^2/K^2, $T = 300$ K, N_C (Si) $= 2.8 \times 10^{19}$ /cm^3.

From the assumption of one-dimensional case and the steady-state condition ($\partial n/\partial t = 0$), it is convenient to rearrange equations (9) and (11) in a form more appropriate for numerical methods, In this work, we only discuss the n-type semiconductor. By combining with Einstein relations, the current density equation (9) may be rewritten as:

$$\frac{dn_s(x)}{dx} + \frac{E(x)}{V_t} n_s(x) = \frac{J_{dn}(x)}{\mu_n kT} \tag{20}$$

which may be treated as a first-order linear differential equation in the unknown $n_s(x)$. If the other terms are non-constant coefficients, then solving this equation for $n_s(x)$ to achieve analytical solution is straightforward:

$$n_s(x) = \exp[-\int \frac{E(x)}{V_t} dx]\ \{ \int [\frac{J_{dn}(x)}{\mu_n kT} \exp(\int \frac{E(x)}{V_t} dx)]\ dx + Cn \} \tag{21}$$

Cn is an integration constant. A more definite form is obtained If x and L are taken as limits of integration and if Cn is expressed in terms of the boundary condition at the point L. By using the basic concept,

$$E(x) = \frac{-d\Psi(x)}{dx} \tag{22}$$

where $\Psi(x) = \phi_{Bn} - \psi(x)$ is the potential distribution, $n_s(x)$ is expressed as:

$$n_s(x) = \exp[\frac{\Psi(x)}{V_t}]\{n_s(L)\exp[-\frac{\Psi(L)}{V_t}] - \int_x^L \frac{J_{dn}(x')}{\mu_n kT}\exp[-\frac{\Psi(x')}{V_t}]dx'\}$$

(23)

Under steady-state conditions, integration of continuity equation (9) yields the current density J_n that may be expressed in terms of U(x),

$$J_n(x) = -q\int_0^x U(x')dx' + J_{dn}(0) \qquad (24)$$

where U(x) = G(x) − R(x) is the effective generation-recombination rate. The integrated constant $J_{dn}(0)$ is obtained by inserting equation (24) into equation (23). Evaluating it at x = 0 and rearranging the terms, we obtain:

$$J_{dn}(0) =$$

$$-q\frac{n_s(0)\exp[-\frac{\Psi(0)}{V_t}] - n_s(L)\exp[-\frac{\Psi(L)}{V_t}] - \{\int_0^L \frac{\exp[\frac{-\Psi(x)}{V_t}]}{V_t\mu_n}[\int_0^x U(x)dx]dx\}}{\frac{1}{V_t\mu_n}\int_0^L \exp[-\frac{\Psi(x)}{V_t}]dx}$$

(25)

According to the assumption of equation (15), equation (25) can be rearranged so that the surface concentration $n_s(0)$ is determined as:

$$n_S(0) =$$

$$\frac{\frac{n_n \nu_R}{V_t \mu_n} \int_0^L \exp[-\frac{\Psi(0)}{V_t}] + n_s(L)\exp[-\frac{\Psi(L)}{V_t}] + \{\int_0^L \frac{\exp[\frac{-\Psi(x)}{V_t}]}{V_t \mu_n} [\int_0^x U(x')dx']dx\}}{\frac{\nu_R}{V_t \mu_n} \int_0^L \exp[-\frac{\Psi(x)}{V_t}]dx + \exp[-\frac{\Psi(0)}{V_t}]} \tag{26}$$

By substituting equations (14), (25), (26) and a set of boundary conditions:

$$n_S(L) = n_0 \exp[\frac{V + \Psi(L) - \Psi(0)}{V_t}], \qquad \Psi(0) \equiv 0$$

into equation (21) and using the limits x_m and w (the width of depletion region of discussed structure) instead 0 and L, the expression for current density follows as:

$$J_n = q\int_0^x U(x')dx' + \frac{q\nu_R}{(1 + \nu_R / \nu_D)V_t \mu_n} \int_{x_m}^{w} \{\exp[-\frac{\Psi(x)}{V_t}][\int_0^x U(x')dx']\}dx$$

$$+ \frac{qN_C \nu_R}{1 + \nu_R / \nu_D} \exp[-\frac{\phi_{Bn}}{V_t}][\exp(\frac{V}{V_t}) - 1] \tag{27}$$

where

$$\nu_D \equiv \{\int_{x_m}^{w} \frac{1}{V_t \mu_n} \exp[-\frac{\Psi(x)}{V_t}]dx\}^{-1} \tag{28}$$

As discussed previously, from equation (6), the potential distribution $\Psi(x)$ can be expressed appropriately as [25]

$$\Psi(x) = Ex + \frac{q}{16\pi\varepsilon_s x} - \Delta\phi \tag{29}$$

and the results of W (depletion width), E(x) and x_m for the metal-semiconductor barrier are similar to those of the one-sided abrupt p^+ -n junction and can be expressed as [25]:

$$W(V) = \{\frac{2\varepsilon_s}{qN_D}[\phi_{Bn} - V - V_t(\ln\frac{N_C}{N_D} + 1)]\}^{1/2} \tag{30}$$

$$E(x) = \frac{qN_D}{\varepsilon_s}(W - x) \tag{31}$$

$$x_m(V) = \frac{1}{4}[\frac{1}{2\pi^2\varepsilon_s^2 N_D}]^{1/4}[\phi_{Bn} - V - V_t(\ln\frac{N_C}{N_D} + 1)]^{-1/4} \tag{32}$$

It can be seen that setting Eq. (30), (31), and (32) into Eq. (27) will make expression (27) more practical for the purposes of numerical calculations. Taking a look at expression (27) closely and carefully, it can be found that the first and second terms of equation (27) obviously are caused by the effect of generation-recombination processes in the space charge region. The third term is exactly the expression represented by Crowell and Sze [5] who were applying the thermionic emission-diffusion theory by introducing the concept of recombination velocity. On the other hand, expression (27) is a theoretical expression because it includes the non-realistic term U(x) for the expression of the generation-recombination process. Before going further to discuss the term U(x) in expression (27), the important parameter for Schottky diode structure should be introduced which is *n*. The *n* is often called the ideality factor and for thermionic emission theory it is defined as [7]

$$1/n = 1 - (\partial\phi_{\mathrm{Bn}} / \partial \mathrm{V}).$$

This concept was mentioned earlier in section 4.2. It has been known that the effective barrier height ϕ_{Bn} is a bias dependent parameter that will cause modifications to the I-V characteristic. If $\partial\phi_{\mathrm{Bn}} / \partial \mathrm{V}$ happens to be constant, *n* is also a constant. But more usually, $\partial\phi_{\mathrm{Bn}} / \partial \mathrm{V}$ is not constant and the ideality factor is generally a function of bias as well. It can only be specified for a particular operating point on the I-V characteristic. The ideality factor *n* is more commonly found in the literature as

$$\frac{1}{\mathrm{n}} = \frac{\mathrm{kT}}{\mathrm{q}}\frac{\mathrm{d}(\ln \mathrm{J})}{\mathrm{dV}} \tag{33}$$

and it can be obtained from the gradient of a graph of lnJ versus voltage. An expression for *n* which is useful over a wider range of voltages than the traditional definition is

$$\frac{1}{\mathrm{n}} = \frac{\mathrm{kT}}{\mathrm{q}}\frac{\mathrm{d}}{\mathrm{dV}}\ln[\frac{\mathrm{J}}{1-\exp(-\frac{\mathrm{qV}}{\mathrm{kT}})}] \tag{34}$$

This equation has the advantage that it may be used for $V < 3kT / q$ and for reverse bias.

The importance of recombination in Si diodes was first demonstrated by Yu and Snow[2], who measured the temperature dependence of the forward current, when recombination current is important. Two activation energies were observed, the first at high temperature due to thermionic emission equal to $[\phi_{Bn} - V]$ and the second at low temperature due to recombination equal to $[(E_g - V) / 2]$. As mentioned in section 4.2, the transport mechanisms of recombination process should yield a similar current voltage relationship as equation (2a) and the recombination current density for low forward bias is given approximately by,

$$J_r = J_{r0} \exp(\frac{qV}{2kT})[1 - \exp(-\frac{qV}{kT})] \tag{35}$$

where $J_{ro} = q\ n_i\ W\ /\ 2\ \tau_r$, n_i is the intrinsic electron concentration, W is the thickness of the depletion region and τ_r is the carrier lifetime within the depletion region. Assuming thermionic-emission theory, the ratio of the thermionic current to the recombination current is given by [7]

$$\frac{2A^{**}T^2\tau_r}{qn_iW} \exp[\frac{q}{2kT}(V - 2\phi_{Bn})]$$

From this expression, it can be seen that recombination is likely to be relatively more important in Schottky structure which have high barriers and the material of low carrier lifetimes, at low temperatures, and at low forward-bias voltage. This actually does not imply that recombination current effect is not important for low barrier height Schottky structures. This is a very important factor for determining the accurate barrier height. The simple result of the expression of recombination current shown above embodies several rather drastic assumptions. The efficiency of a recombination center depends on its ability to capture both majority and minority carriers. The recombination rate is maximum when the center lies at mid gap as this is the position that maximizes the probability for both processes. If the electron and hole capture cross sections can be considered to be equal, it can be shown that the presence of a mid-gap recombination center leads to a recombination current which is proportional to [exp (qV / 2kT) – 1] [1]. However, none of these assumptions are likely to be true in practice, especially, the equality of the electron and hole capture cross-sections, which may differ by as much as three orders of magnitude. Sah, Noyce, and Shockley [41] have shown that, depending on the ratio of the capture cross-sections, the value of *n* for recombination current may be between 1 and 2. The simple expression for recombination current density J_r for low forward bias is therefore a gross simplification. This is given approximately by the formula of current density (35). If one accepts the equation (35), the generation-recombination term in equation (27) can be written in the form:

$$J_r = q\int_0^x U(x')dx' = J_{r0}\exp\left(\frac{qV}{2kT}\right)\left[1-\exp\left(-\frac{qV}{kT}\right)\right] \qquad (36)$$

The factor of two in exponent arises directly from the assumption that the product *pn* is described by a function of form $pn = n_i^2 \exp(qV/kT)$ where *p* is the hole concentration and *n* is the electron concentration. This is equivalent to assuming that the hole and electron non-equilibrium quasi-Fermi energies are flat and separated by qV throughout the depletion region. The recombination centers provide a parallel conduction path and the I-V characteristics contain an additional component. Now, the total current / voltage expression (27) can therefore be written as:

$$J_n = J_r\left(1+\frac{v_R / v_D}{1+v_R / v_D}\right)+\frac{qN_C v_R}{1+v_R / v_D}\exp\left[-\frac{\phi_{Bn}}{V_t}\right]\left[\exp\left(\frac{V}{V_t}\right)-1\right] \tag{37}$$

Equation (37) is only a good description of the transport properties for moderately doped metal-semiconductor.

The physical structures of the samples fabricated in this work suggested the partitioning of the structure model into two components: the Schottky barrier and silicon depletion region; the substrate and back contact. The sample #1 was fabricated by using front 3000Å of Al-1%Si (wt%) on top of 3000Å Ti_{03} W_{07} (10: 90 wt%) contacted with (100) orientation n-type Si, and 3000Å Al-1%Si (wt%) on the back of silicon substrate. The sample #2 was made by using 3000Å $Ti_{03}W_{07}$ (10:90 wt%) contact to (100) orientation n-type Si and 3000Å Al-1%Si (wt%) on the back of silicon substrate. Details about the fabrication of the devices used in this work will be given in the next section. The sample structures are showed in Fig.5.

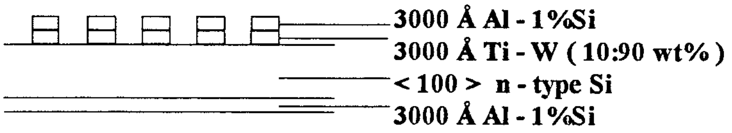

(a) Sample #1 Al(1%Si)/$Ti_{03}W_{07}$/n-Si/Al(1%Si).

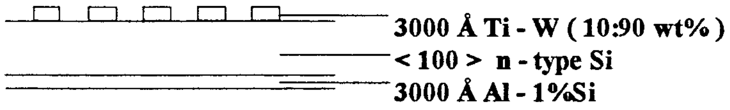

(b) Sample #2 $Ti_{03}W_{07}$/n-Si/Al(1%Si).

Fig.5 The schematic diagrams of experimental Schottky structures for measurements.

A logarithmic plot of I/[1−exp(−qV/kT)] versus voltage to describe the I-V characteristic for the thermionic-emission model should be a straight line. However, the recombination current is a common cause of departure from this ideal behavior in Schottky diodes at low forward bias and the series resistance is another reason causing the graph to be non-linear. In order to consider the distribution of series resistance, the voltage V in the equation (37) should be replaced by the term (V_a − IR), here, R is the series resistance. After taking the term (V_a − IR) instead of V, equation (37) becomes to

$$I = I_r (1 + \frac{v_R / v_D}{1 + v_R / v_D}) + \frac{qN_C v_R}{1 + v_R / v_D} \exp[-\frac{q\phi_{Bn}}{kT}]\{\exp[\frac{q(V_a - IR)}{kT}] - 1\} \tag{38}$$

where

$$I_r = \frac{qn_i WS}{2\tau_r} \exp[\frac{q(V_a - IR)}{2kT}]\{1 - \exp[-\frac{q(V_a - IR)}{kT}]\} \tag{39}$$

In actual calculations, equation (38) will be used to fit experimental data. This expression describes not only the thermionic-emission/drift-diffusion current, but also the generation-recombination current. For the Schottky structures used in this study Al(1%Si)/$Ti_{03}W_{07}$/n-Si/Al(1%) and $Ti_{03}W_{07}$/n-Si/Al(1%), the effective barrier height ϕ_{Bn}= 0.554eV and 0.519eV respectively are obtained from the experimental I-V measurements. Other relevant data is shown in Table 1

The procedure for calculations of I-V characteristics is completed by using the software package mathematica and the calculated results are given in the Appendix A. Fig.6 shows the calculation procedure. The calculated results of I-V characteristics are plotted in Figs. 7-11 for samples #1 and #2 respectively.

Table 1. Data for calculations of the I-V characteristics.

effective barrier height	barrier height lowering	electron doping concen-tration	carrier lifetime	thickness of depletion region	location of lowering	series resistance
ϕ_{Bn} (eV)	$\Delta\phi$ (eV)	N_D(cm^{-3})	τ_r (s)	W (cm)	x_m (cm)	R (Ω)
sample #1 0.554	0.018 → 0.007	10^{15}	5E-11	3.604E-5 → 5.132E-6	3.909E-7 → 8.805E-7	20
sample #2 0.519	0.018 → 0.006	10^{15}	4E-11	2.579E-5 → 3.647E-6	3.929E-7 → 1.066E-6	60
	equation (17)		fit	equation (30)	equation (32)	fit

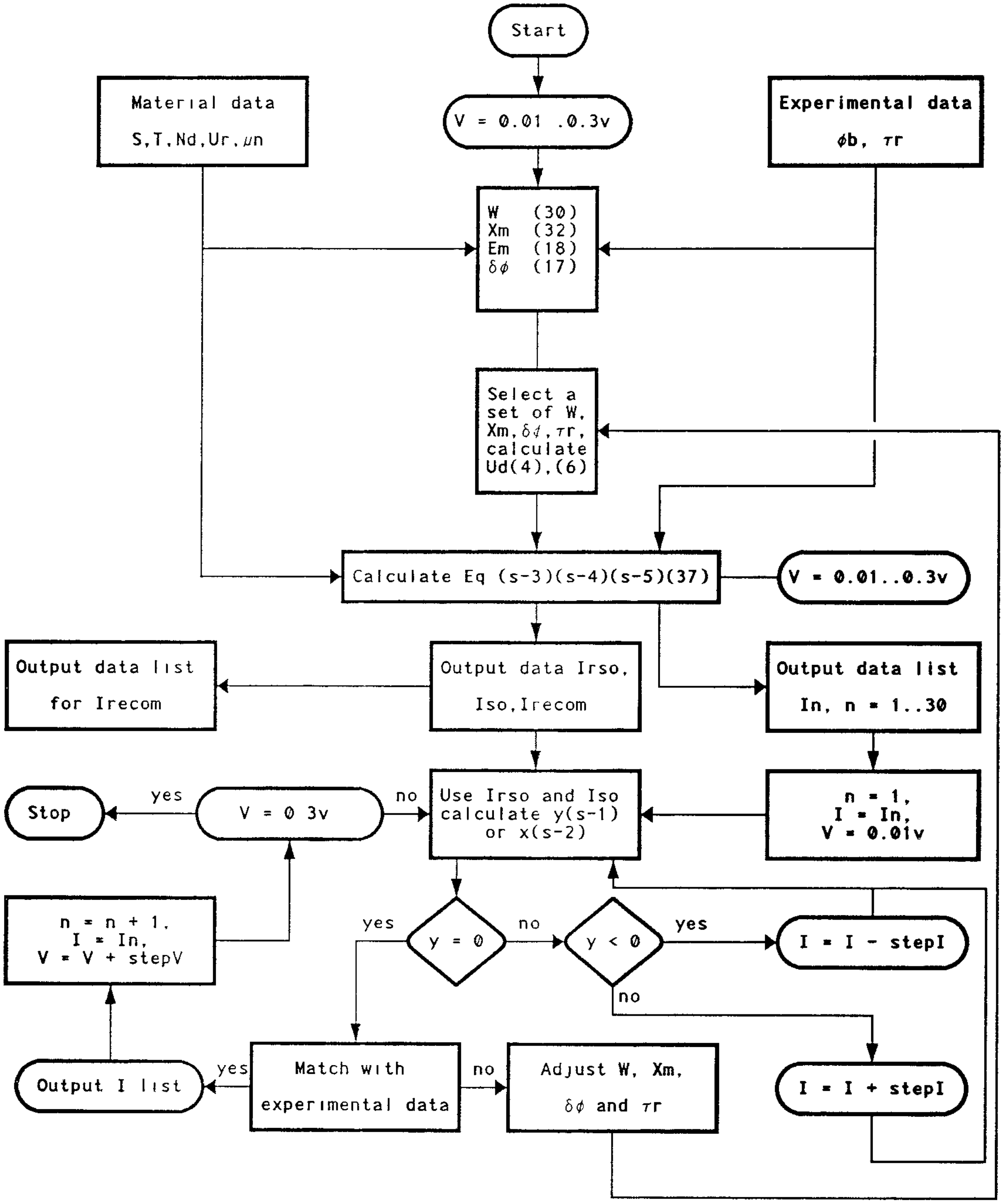

Fig.6 Flow chart of the calculation procedure. The numbers within the parentheses are the equation numbers in this thesis (all equtions are shown in Appendix C).

The results of the calculations are given in the Appendix A. From Fig. 6-10, it is seen that the effect of recombination current is relatively more important for the low forward bias voltage region even for the relatively low barrier height devices (0.554eV and 0.519eV). In fact, it is expected that the effect of recombination current is not significantly large for the devices used in this study. Shortly it will be seen that the expression (38) approached by using the derivative procedure, described in this section, is more accurate to describe the current transport properties than the traditional thermionic-emission/drift-diffusion model. The calculated results will be compared with experimental results in the next section to further illustrate the accuracy of using expression (38). Actually, the influence of recombination current can also be seen in the data sheet attached on Appendix A.

The importance of recombination current in causing small departures from ideal behavior has been frequently overlooked in the literature. It is necessary to derive a more accurate expression to describe the I-V characteristics of metal-semiconductor contacts. Earlier studies have demonstrated that the recombination current is most important for low forward voltages and the neglect of electron recombination in the analysis of the I-V curves of moderately doped Schottky structures will lead to a false extrapolated value of J_s (saturation current). This leads to systematic error in the value of the barrier height. By taking recombination current into account, explicitly an accurate value of the barrier height can be obtained.

On the other hand, it is a more frequently used method to extrapolate the value of the effective barrier height from graphs of lnJ versus V with the ideality factor *n* greater than one. Brillson (1981) has stated that 'extrapolating lnJ to zero applied voltage in order to obtain barrier height is not a reliable procedure for devices with values of *n* significantly different from one'. This is because the transport processes which cause deviation from 'ideal' behavior have to be more accurately described if reliable estimates of barrier height are to be made. Several laboratories (e.g. Mclean, Dharmadasa, and Williams, 1986) have developed computer programs which use a curve-fitting technique to obtain values of the parameters J_s and R which best represent the experimental I-V characteristics, thus enabling reliable values of effective barrier height ϕ_{Bn} to be obtained.

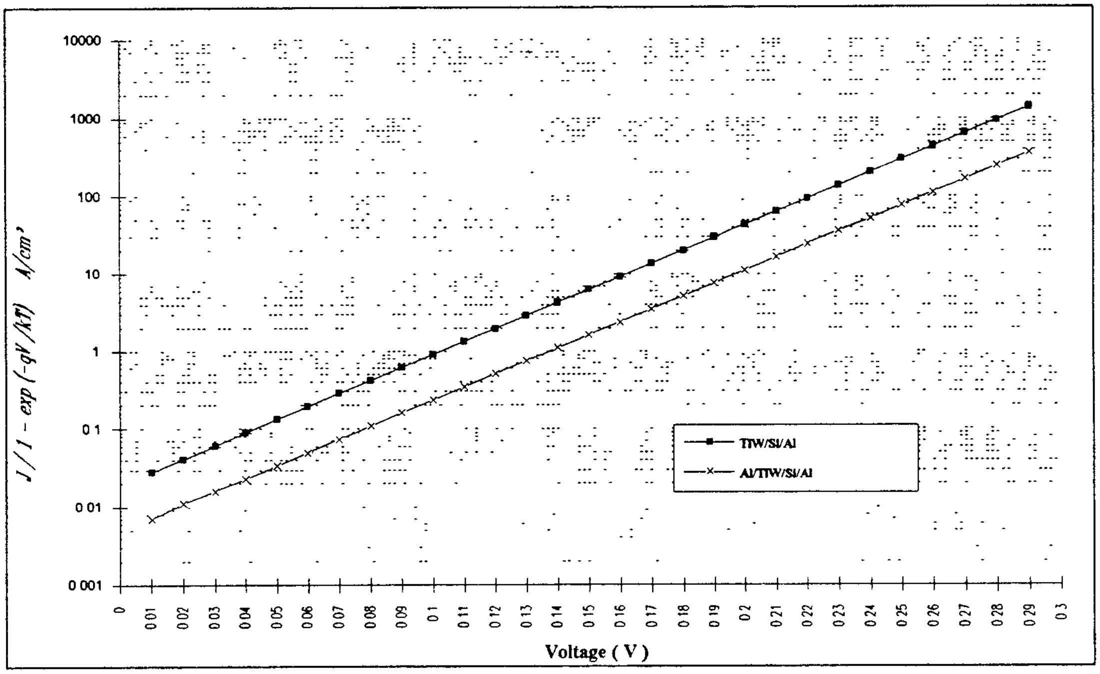

Fig.7 Calculated by using the ideal I-V characteristic model under forward bias for samples #1 and #2.

Sample #1: Al/TiW/n-Si/Al. Sample #2: TiW/n-Si/Al.

Recombination current and series resistance are considered to be zero. The calculation equation is:

$$J_n = [A^{**}T^2 \exp(-\frac{q\phi_{Bn}}{kT})][\exp(\frac{qV}{kT}) - 1] = J_{ST}[\exp(\frac{qV}{kT}) - 1]$$

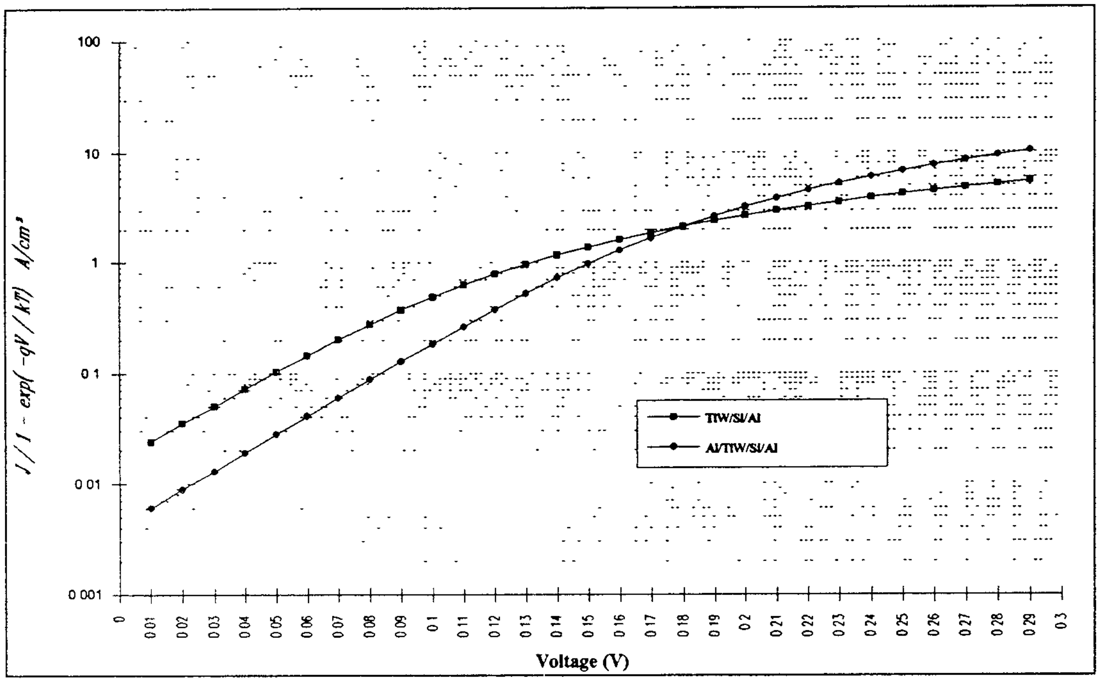

Fig.8 Calculated by using Crowell and Sze's theory without the effect of recombination but with series resistance for samples #1 and #2.

Sample #1: Al/TiW/n-Si/Al. Sample #2: TiW/n-Si/Al.

The calculation equation is:

$$J = \frac{qN_c v_R}{1 + v_R/v_D} \exp(-\frac{q\phi_{Bn}}{kT})\{\exp[\frac{q(V_a - IR)}{kT}] - 1\}$$

where

$$v_D \equiv \{\int_{x_m}^{W} \frac{q}{\mu_n kT} \exp[-\frac{q}{kT}(\phi_{Bn} - \psi)]dx\}^{-1}$$

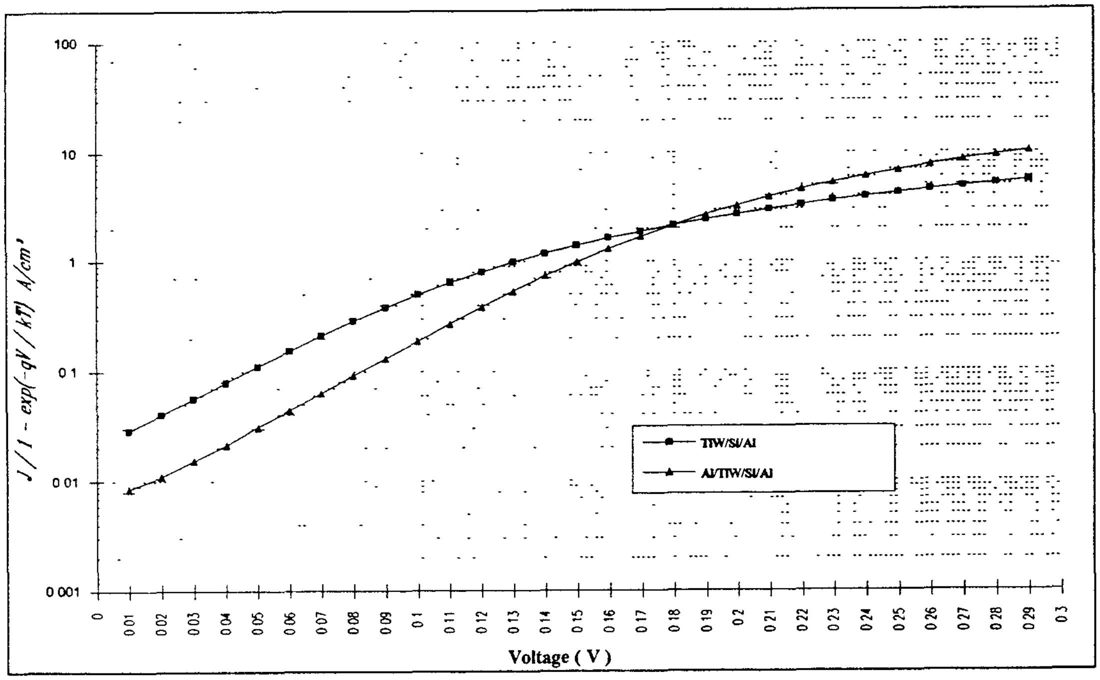

Fig.9 Calculated by using Eq. (38) for the I-V characteristics. This includes the influence of recombination and series resistance for samples #1 and #2.

Sample #1: Al/TiW/n-Si/Al. Sample #2: TiW/n-Si/Al.

The calculation equation is:

$$I = I_r\,(1 + \frac{v_R / v_D}{1 + v_R / v_D}) + \frac{qN_C v_R}{1 + v_R / v_D}\exp[-\frac{q\phi_{Bn}}{kT}]\{\exp[\frac{q(V_a - IR)}{kT}] - 1\}$$

where

$$I_r = \frac{qn_i WS}{2\tau_r}\exp[\frac{q(V_a - IR)}{2kT}]\{1 - \exp[-\frac{q(V_a - IR)}{kT}]\}$$

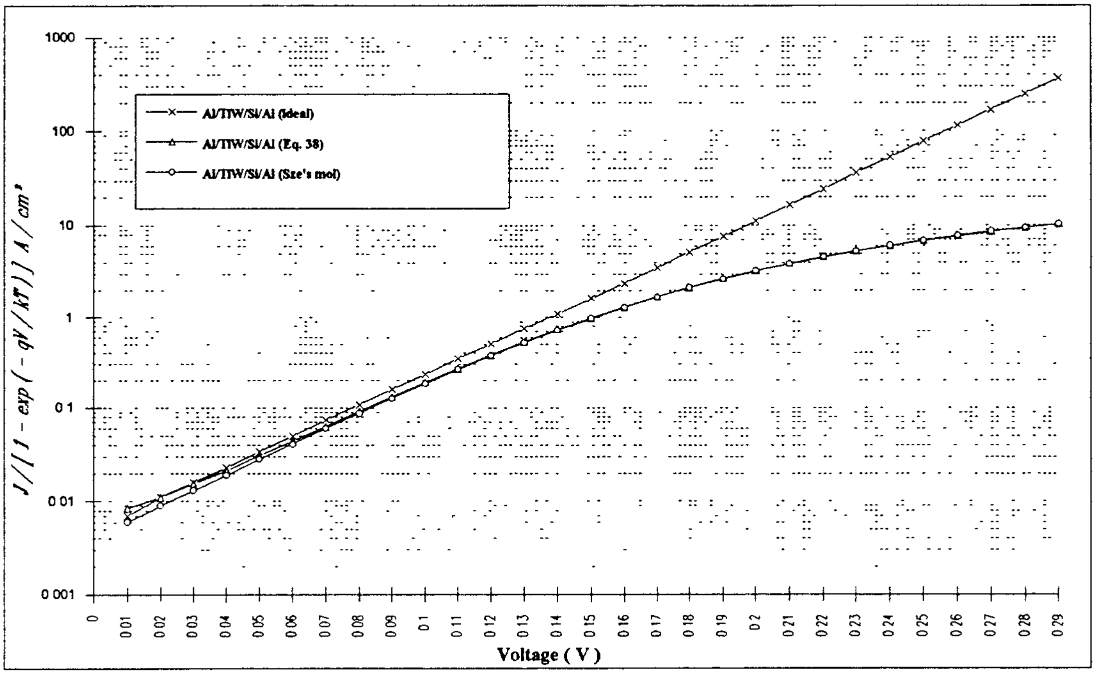

Fig.10 Calculated from the different models for sample #1 (Al/TiW/n-Si/Al). Ideal model without recombination and series resistance:

$$J_n = [A^{**}T^2 \exp(-\frac{q\phi_{Bn}}{kT})][\exp(\frac{qV}{kT}) - 1] = J_{ST}[\exp(\frac{qV}{kT}) - 1]$$

Crowell and Sze' model with series resistance, without recombination:

$$J = \frac{qN_c v_R}{1 + v_R/v_D} \exp(-\frac{q\phi_{Bn}}{kT})\{\exp[\frac{q(V_a - IR)}{kT}] - 1\}$$

where

$$v_D \equiv \{\int_{x_m}^{W} \frac{q}{\mu_n kT} \exp[-\frac{q}{kT}(\phi_{Bn} - \psi)]dx\}^{-1}$$

Equation (38) with recombination and series resistance:

$$I = I_r(1 + \frac{v_R / v_D}{1 + v_R / v_D}) + \frac{qN_C v_R}{1 + v_R / v_D} \exp[-\frac{q\phi_{Bn}}{kT}]\{\exp[\frac{q(V_a - IR)}{kT}] - 1\}$$

where

$$I_r = \frac{qn_i WS}{2\tau_r} \exp[\frac{q(V_a - IR)}{2kT}]\{1 - \exp[-\frac{q(V_a - IR)}{kT}]\}$$

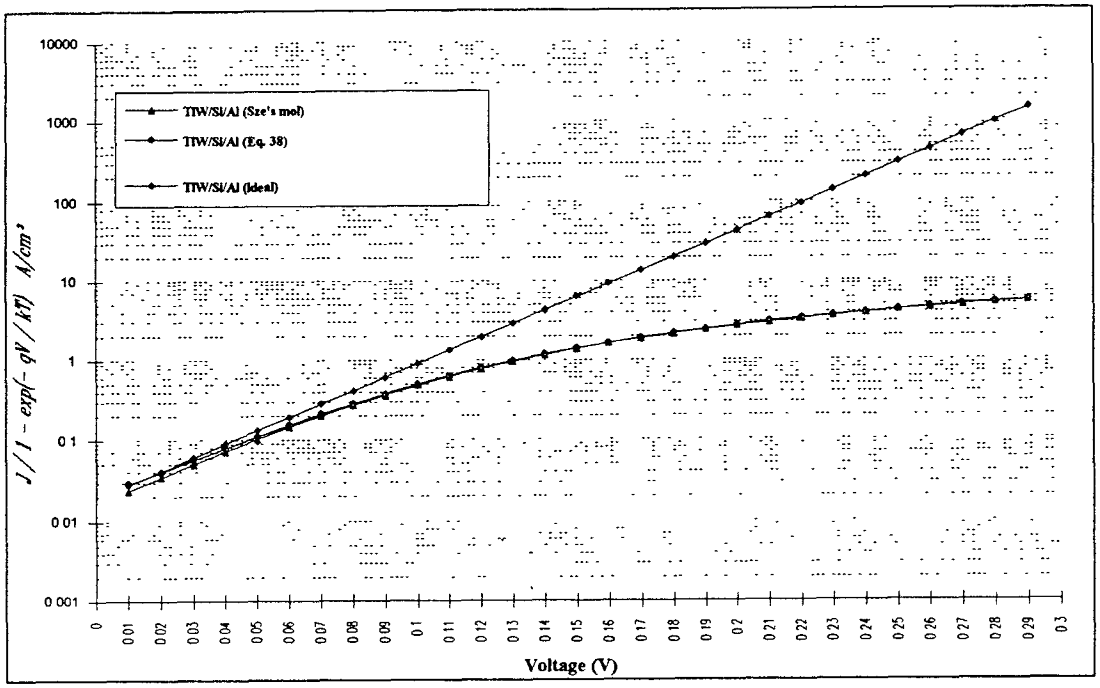

Fig.11 Calculated from the different models for sample #2 (TiW/n-Si/Al). Ideal model without recombination and series resistance:

$$J_n = [A^{**}T^2 \exp(-\frac{q\phi_{Bn}}{kT})][\exp(\frac{qV}{kT}) - 1] = J_{ST}[\exp(\frac{qV}{kT}) - 1]$$

Crowell and Sze' model with series resistance, without recombination:

$$J = \frac{qN_c v_R}{1 + v_R/v_D} \exp(-\frac{q\phi_{Bn}}{kT})\{\exp[\frac{q(V_a - IR)}{kT}] - 1\}$$

where

$$v_D \equiv \{\int_{x_m}^{W} \frac{q}{\mu_n kT} \exp[-\frac{q}{kT}(\phi_{Bn} - \psi)]dx\}^{-1}$$

Equation (38) with recombination and series resistance:

$$I = I_r(1 + \frac{v_R / v_D}{1 + v_R / v_D}) + \frac{qN_C v_R}{1 + v_R / v_D} \exp[-\frac{q\phi_{Bn}}{kT}]\{\exp[\frac{q(V_a - IR)}{kT}] - 1\}$$

where

$$I_r = \frac{qn_i WS}{2\tau_r} \exp[\frac{q(V_a - IR)}{2kT}]\{1 - \exp[-\frac{q(V_a - IR)}{kT}]\}$$

4.4 I-V Method of Experimental Measurements of Barrier Heights

Sample #1 was prepared by sputter deposition of 3000Å of Al(1%Si) on top of 3000Å W-10%Ti (90:10 wt%) alloy films on 4-inch n-type (100) oriented Si wafer with 10 Ω-cm resistivity. 3000 Å Al(1%Si) contact was made on the back of Si. After conventional masking and wet etching, well defined metal patterns on the front were obtained. The area of the pattern is 4.22×10^{-4} cm^2.

Sample #2 was prepared by sputter deposition of 3000Å W-10%Ti (90:10 wt%) alloy films on 4-inch n-type (100) oriented silicon wafer with 10 Ω-cm resistivity, 3000 Å Al(1%Si) contact was made on the back of silicon. The area of the devices is 7.51×10^{-4} cm^2.

Each sample consisted of 2000 devices. The results in this study represent an average of 200 measurements per sample. Barrier height for these samples were determined by extrapolating the dark forward I-V characteristics to zero applied voltage to obtain the saturation current J_S. The barrier height is obtained from the equation,

$$\phi_{Bn} = \frac{kT}{q} \ln\left(\frac{A^{**}T^2}{J_s}\right) \tag{40}$$

The extrapolation was made by a linear fit over two orders of magnitude or greater of current on the semilog I-V characteristics. The effective Richardson's constant was taken to be 110 A/K^{2}cm^2 for electrons. The slope of the linear portion yielded the value of the ideality factor *n* expressed by the equation

$$\frac{1}{n} = \frac{kT}{q} \frac{d(\ln J)}{dV} \tag{41}$$

The measurements were made on samples at room temperature. The measured results are listed in Table 2.

Table 2 Data obtained from I-V characteristics.

	barrier height ϕ_{Bn} (eV) I-V	barrier height ϕ_{Bn} (eV) Norde [31]	ideality factor n
sample #1	0.5544	0.5614	1.065
sample #2	0.5185	0.5229	1.13

The measured results of forward and reverse I-V characteristics are plotted in Figs.12-15 respectively. The comparison of the experimental I-V characteristics with calculated results by using Eq. (38) is given in Figs. 16 and 17.

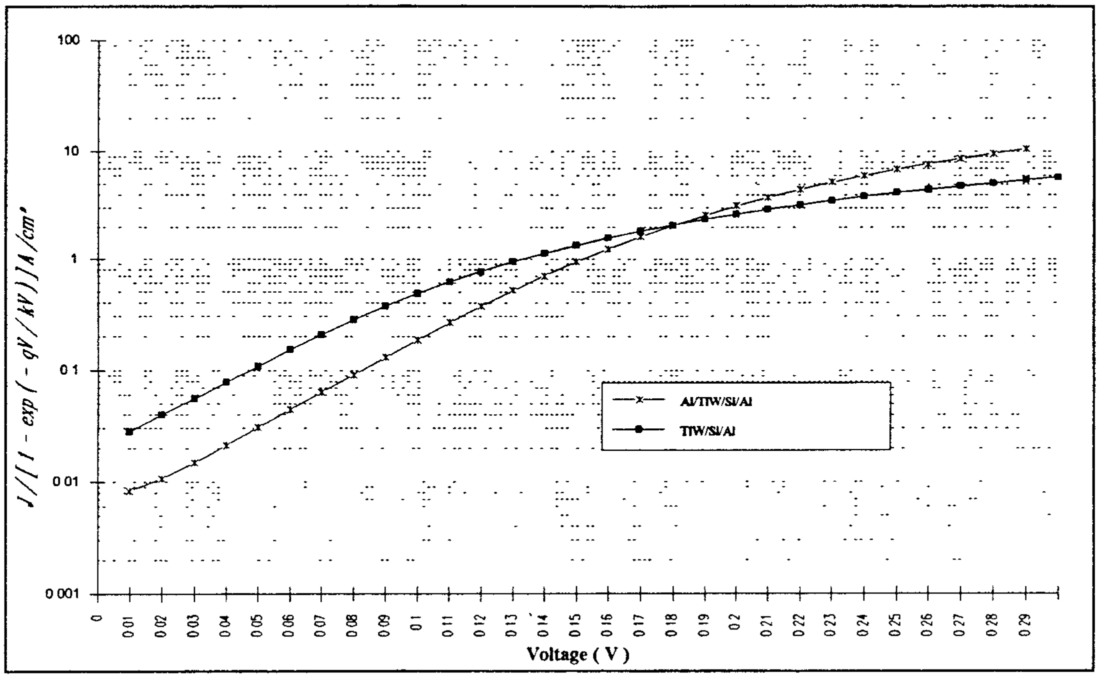

Fig. 12 Plot the experimental results of forward I-V characteristics by using J/1-exp(-qV/kT) vs. V for samples #1 and #2.

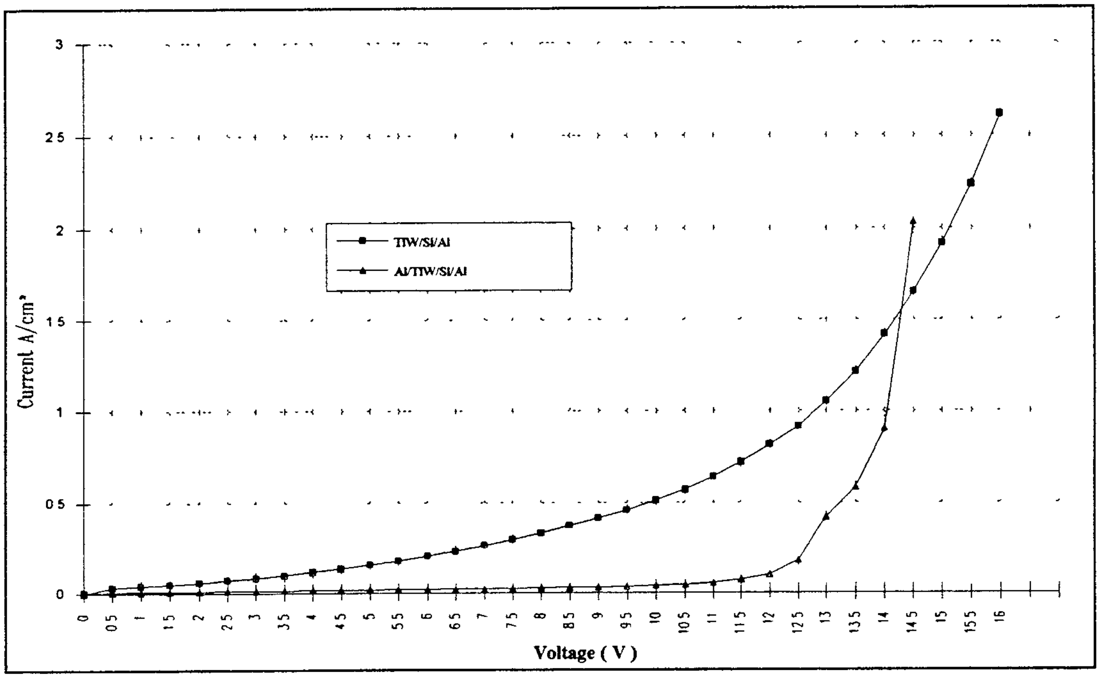

Fig. 13 Experimental results of reverse I-V characteristics for samples #1 and #2. Sample #1: Al/TiW/n-Si/Al. Sample #2: TiW/n-Si/Al. (measured data is listed in Appendix B)

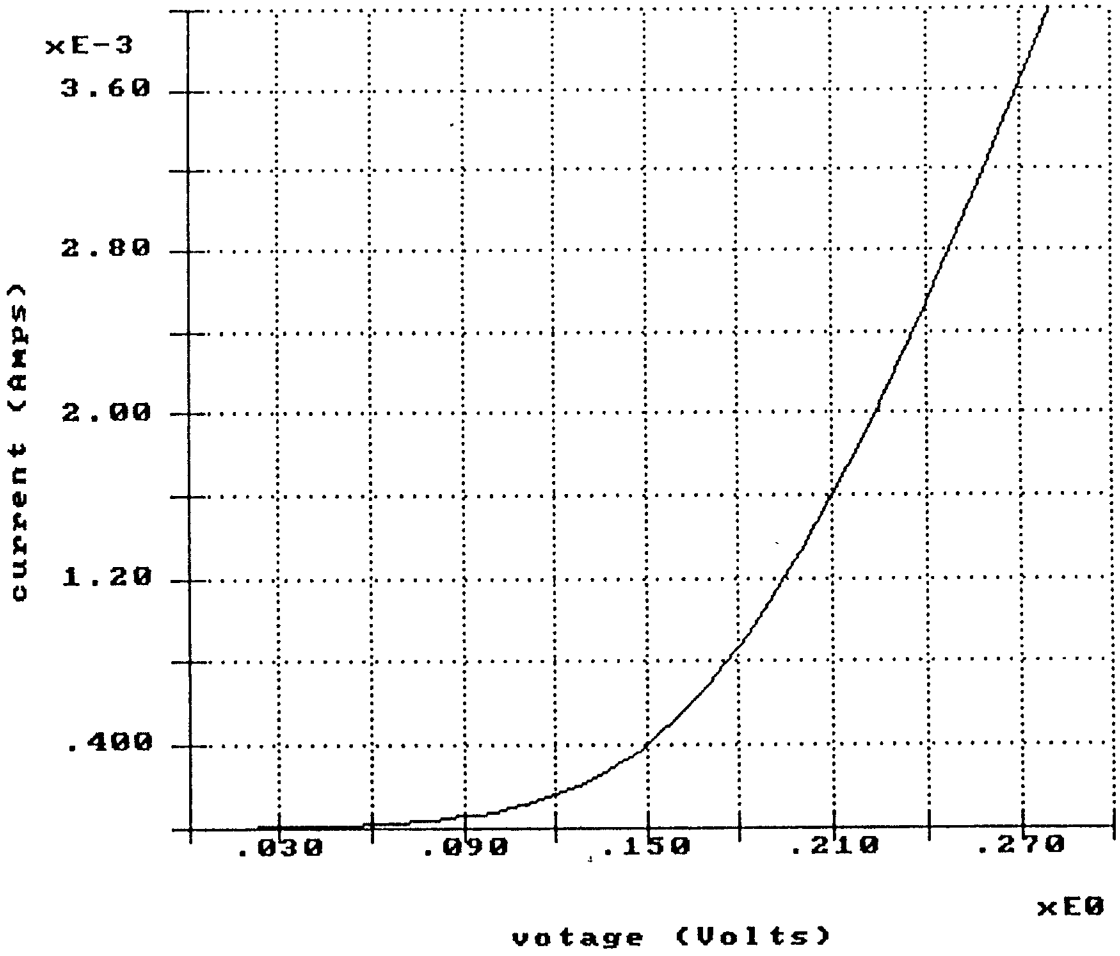

Fig.14 Experimental result of forward I-V characteristics for sample #1 (Al/TiW/n-Si/Al)

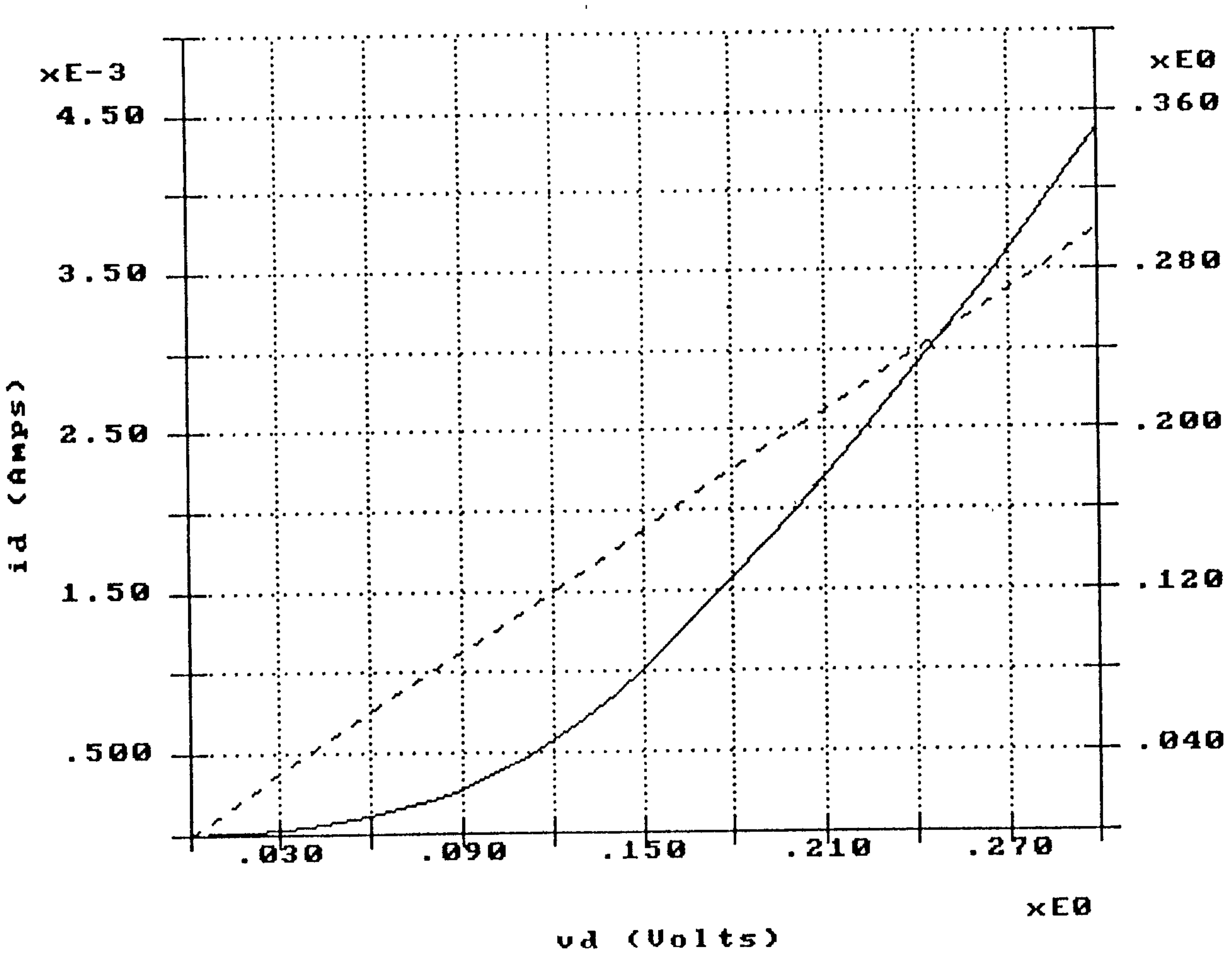

Fig.15 Experimental result of forward I-V characteristics for sample #2 (TiW/n-Si/Al).

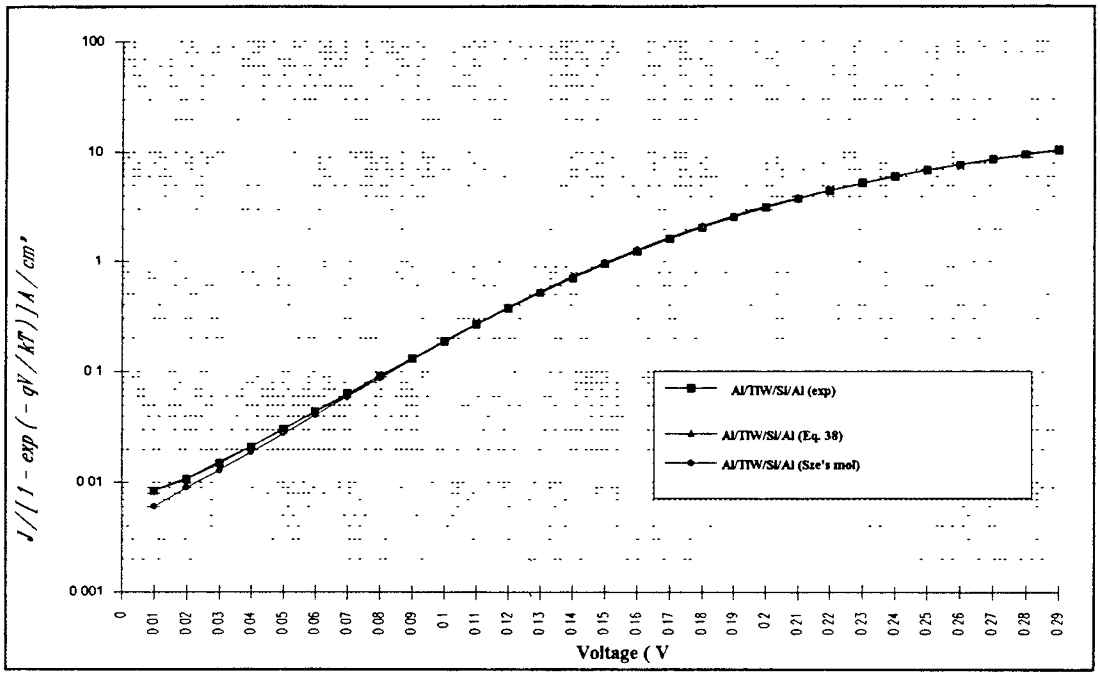

Fig.16 Comparison between experimental and calculated I-V characteristics. Sample #1(Al/$Ti_{0.3}W_{0.7}$/n-Si/Al).

Crowell and Sze' model with series resistance, without recombination:

$$J = \frac{qN_c v_R}{1 + v_R/v_D} \exp(-\frac{q\phi_{Bn}}{kT})\{ \exp[\frac{q(V_a - IR)}{kT}] - 1\}$$

where

$$v_D \equiv \{ \int_{x_m}^{W} \frac{q}{\mu_n kT} \exp[-\frac{q}{kT}(\phi_{Bn} - \psi)]dx\}^{-1}$$

Equation (38) with recombination and series resistance:

$$I = I_r (1 + \frac{v_R / v_D}{1 + v_R / v_D}) + \frac{qN_C v_R}{1 + v_R / v_D} \exp[-\frac{q\phi_{Bn}}{kT}]\{\exp[\frac{q(V_a - IR)}{kT}] - 1\}$$

where

$$I_r = \frac{qn_i WS}{2\tau_r} \exp[\frac{q(V_a - IR)}{2kT}]\{1 - \exp[-\frac{q(V_a - IR)}{kT}]\}$$

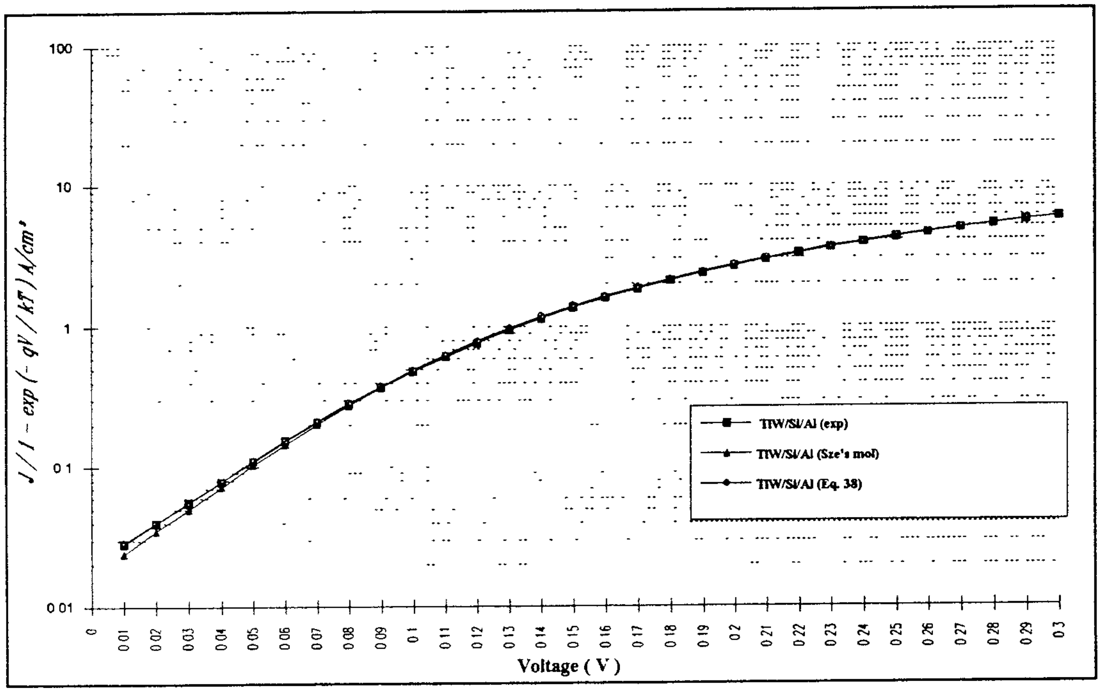

Fig. 17 Comparison between experimental and calculation I-V characteristics. Sample #2 ($Ti_{0.3}W_{0.7}$/n-Si/Al).

Crowell and Sze' model with series resistance, without recombination:

$$J = \frac{qN_c v_R}{1 + v_R/v_D} \exp\left(-\frac{q\phi_{Bn}}{kT}\right)\left\{\exp\left[\frac{q(V_a - IR)}{kT}\right] - 1\right\}$$

where

$$v_D \equiv \left\{\int_{x_m}^{W} \frac{q}{\mu_n kT} \exp\left[-\frac{q}{kT}(\phi_{Bn} - \psi)\right] dx\right\}^{-1}$$

Equation (38) with recombination and series resistance:

$$I = I_r\left(1 + \frac{v_R / v_D}{1 + v_R / v_D}\right) + \frac{qN_C v_R}{1 + v_R / v_D} \exp\left[-\frac{q\phi_{Bn}}{kT}\right]\left\{\exp\left[\frac{q(V_a - IR)}{kT}\right] - 1\right\}$$

where

$$I_r = \frac{qn_i WS}{2\tau_r} \exp\left[\frac{q(V_a - IR)}{2kT}\right]\left\{1 - \exp\left[-\frac{q(V_a - IR)}{kT}\right]\right\}$$

In Figs. 16 and 17, the calculated and experimentally obtained forward I-V characteristics on samples Al/$Ti_{03}W_{07}$/n-Si/Al and $Ti_{03}W_{07}$/n-Si/Al are presented. The results from calculation of using equation (38) and from experimental measurements are quite identical, and illustrate abundantly the accuracy of equation (38) to describe the I-V characteristics for moderately doped Schottky structures with the effect of generation-recombination in the depletion region. The Crowell and Sze's theory has a difficulty to fit the experimentally measured characteristics under the low forward bias region.

In general, the diodes are always less ideal, and the experimental plots will often show noticeable deviations from linearity. The determination of barrier height from I-V characteristics is only reliable if one can be confident that the current is determined by the thermionic emission theory. For this to be so, the forward portion of the characteristics must be a good straight line over more than one decade, with a low value of n, say at least $n < 1.1$. However, this is only an ideal case. For large values of n, or for non-linear characteristics, the diode is far from ideal, probably due to the presence of a thick interfacial layer which has been studied by many people, or to recombination in the depletion region which has been the focus of this work, and to the effect of series resistance. Because of all of these reasons, it is not possible to determine the current simply from the thermionic emission theory.

From this study, we have seen that the series resistance shows some contribution to the I-V characteristics. This is always the case for real devices. Problems arise if it is necessary to extract reliable values of effective barrier height when the sample has a large series resistance. In that case, the linear interval of the plot of lnJ versus V will be too small to give a reliable value of saturation current extrapolated to zero. A modified forward I-V plot for Schottky diodes with high series resistance has been presented by Norde [31]. Because of the recombination current effct, it is very limited to use this method [32]. In this method, I-V relationship is represented by the function,

$$F(V) = \frac{V}{2} - \frac{kT}{q}\ln\left(\frac{I}{SA**T^2}\right) \tag{42}$$

where S is the diode area. Norde represented that the barrier height can be expressed as,

$$\phi_{Bn} = F(V_0) + \frac{V_0}{2} - \frac{kT}{q} \tag{43}$$

where the value of V_0 is the voltage corresponding to the minimum ($dF/dV = 0$). By using the data measured from I-V, F (V) plots for samples #1 and #2 used in this work are shown in Fig. 18.

In Fig. 18, arrow1 and arrow2 represent the values of V_0 and $F(V_0)$. Using the measured values of I_0, V_0 and $F(V_0)$, we can estimate the series resistance by the following expression

$$R = \frac{kT}{qI_0} \tag{44}$$

The effective barrier heights from this method are greater than the values obtained by extrapolation from I-V. The comparison is shown in table 2. This is because this method is based on the assumptions of neglecting the voltage dependence of barrier height. It does not consider the effect of recombination current at the low forward bias region.

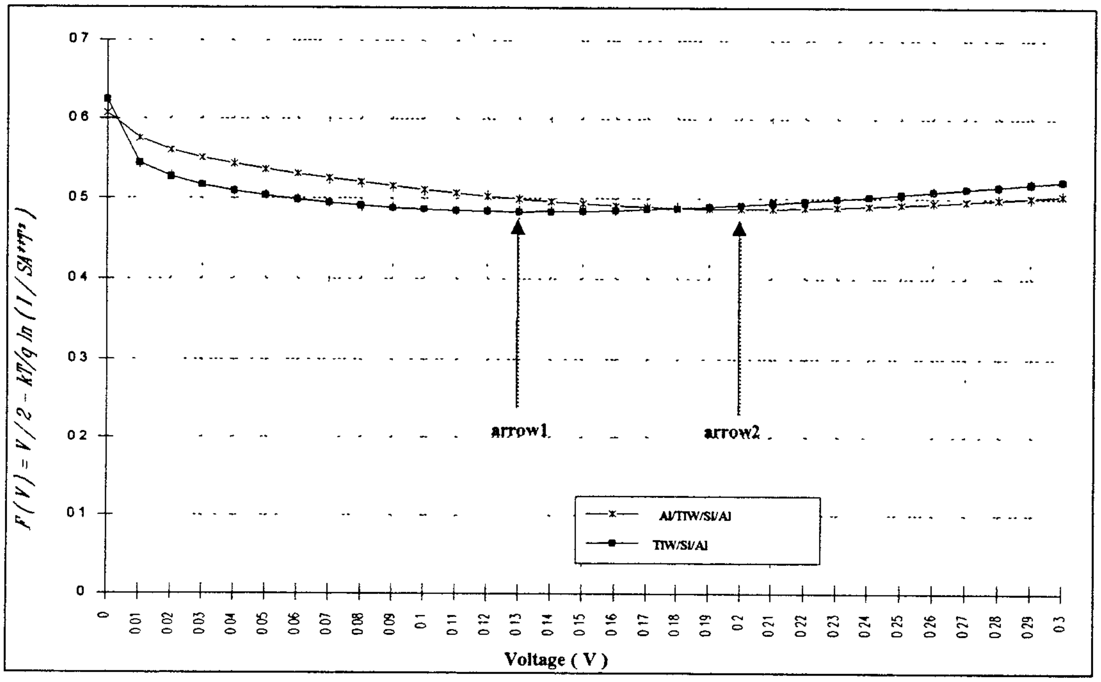

Fig.18 The Norde plot for the modified forward I-V characteristics of samples #1and #2 (I-V data is listed in Appendix B).

Sample #1: Al/$Ti_{0.3}W_{0.7}$/n-Si/Al. Sample #2: $Ti_{0.3}W_{0.7}$/n-Si/Al.

Norde's equation is:

$$F(V) = \frac{V}{2} - \frac{kT}{q}\ln\left(\frac{I}{SA^{**}T^2}\right)$$

CHAPTER 5

SUMMARY

The properties of current transport through Schottky contacts are very important and fundamental in microelectronics. We have investigated the I-V characteristics of moderately doped $Ti_{03}W_{07}$/n-Si/Al and Al/$Ti_{03}W_{0.7}$/n-Si/Al Schottky structures which exhibit non-ideal behavior at room temperature with ideality factors of 1.13 and 1.065 respectively. The Schottky-barrier heights for the $Ti_{03}W_{07}$/n-Si/Al and Al/$Ti_{03}W_{07}$/n-Si/Al, as measured using the linear approximation are in good agreement with the results which describe Ti-W /Si contact structure as low barrier height device.

An accurate model for describing the process of current transport across the rectifying metal semiconductor interface has been presented. The derived final expression of properties for current flow, equation (38), takes into account not only the thermionic-emission/drift-diffusion processes but also the generation-recombination effect within the space charge region. The derived procedure is quite similar to the work has been done for *p-n* junctions and is based on the fundamental equations such as Poisson, current-density and continuity equations. The main difference is solving these equations without making many simplifications or approximations so that it is more accurate than the traditional theoretical expressions.

From the derived current transport expressions, we can use numerical methods to estimate the actual effect of the recombination current which contributes to the I-V characteristics and the magnitude of barrier height. By introducing the generation-recombination mechanisms, this numerical method gives a more complex view of the transport processes and enables a better fit with experimental characteristics in the entire range of applied voltages. We have shown this result by using the more common and typical Schottky structures of $Ti_{03}W_{07}$/n-Si/Al and Al/$Ti_{03}W_{07}$/n-Si/Al which have low barrier height and do not have significant recombination current effects. This result, Eq.(38), can be used for any other Schottky structures.

APPENDIX A

The calculated data sheet

	SAMPLE #1			SAMPLE #2		
$V_{applied}$	J_{expre}	J_{calcu}	J_{recomb}	J_{expre}	J_{calcu}	J_{recomb}
0						
0.01	0.008357	0.0085	1.405e-7	0.028195	0.029	6.023e-7
0.02	0.010736	0.011	2.863e-7	0.03985	0.04	1.227e-6
0.03	0.014886	0.0154	4.429e-7	0.0557	0.56	1.898e-6
0.04	0.021238	0.0212	6.19e-7	0.078493	0.079	2.64e-6
0.05	0.030526	0.031	8.122e-7	0.108597	0.111	3.481e-6
0.06	0.044123	0.044	1.039e-6	0.152971	0.155	4.453e-6
0.07	0.063548	0.063	1.305e-6	0.208768	0.213	5.591e-6
0.08	0.091644	0.092	1.619e-6	0.82029	0.288	6.939e-6
0.09	0.131007	0.132	1.994e-6	0.372639	0.383	8.548e-6
0.10	0.186576	0.19	2.444e-6	0.485007	0.5	1.048e-5
0.11	0.265384	0.27	2.986e-6	0.617781	0.639	1.28e-5
0.12	0.372125	0.382	3.64e-6	0.77142	0.8	1.56e-5
0.13	0.516256	0.533	4.43e-6	0.984812	0.981	1.899e-5
0.14	0.704635	0.733	5.386e-6	1.142272	1.183	2.308e-5
0.15	0.948726	0.99	6.545e-6	1036278	1.401	2.805e-5
0.16	1.251911	1.31	7.948e-6	1.592762	1.636	3.406e-5
0.17	1.624187	1.696	9.65e-6	1.839934	1.885	4.136e-5
0.18	2.062807	2.15	1.171e-5	2.097754	2.146	5.02e-5
0.19	2.577509	2.669	1.422e-5	2.369545	2.418	6.093e-5
0.20	3.152107	3.248	1.725e-5	2.650223	2.699	7.394e-5
0.21	3.792611	3.883	2.093e-5	2.941506	2.989	8.972e-5
0.22	4.48433	4.568	2.54e-5	3.24018	3.285	1.089e-4
0.23	5.234377	5.297	3.082e-5	3.547166	3.591	1.321e-4
0.24	6.02133	6.065	3.74e-5	3.858322	3.9	1.603e-4
0.25	6.856365	6.868	4.538e-5	4.178967	4.215	1.945e-4
0.26	7.720716	7.701	5.506e-5	4.500303	4.535	2.36e-4
0.27	8.622768	8.56	6.68e-5	4.829916	4.859	2.863e-4
0.28	9.54806	9.443	8.105e-5	5.162873	5.187	3.474e-4
0.29	10.50441	10.346	9.834e-5	5.499303	5.517	4.214e-4

$V_{applied}$: experimental applied voltage values

J_{expre}: experimental values of current density

J_{calcu}: calculated values of current density. Calculated by equation (38):

$$I = I_r(1 + \frac{\nu_R / \nu_D}{1 + \nu_R / \nu_D}) + \frac{qN_C\nu_R}{1 + \nu_R / \nu_D} \exp[-\frac{q\phi_{Bn}}{kT}]\{\exp[\frac{q(V_a - IR)}{kT}] - 1\}$$

where

$$I_r = \frac{qn_i WS}{2\tau_r} \exp[\frac{q(V_a - IR)}{2kT}]\{1 - \exp[-\frac{q(V_a - IR)}{kT}]\}$$

J_{recomb}: calculated values of current density. Calculated by equation:

$$I_{reco} = \frac{qn_i WS}{2\tau_r} \exp[\frac{q(V_a - IR)}{2kT}]\{1 - \exp[-\frac{q(V_a - IR)}{kT}]\}(1 + \frac{\nu_R/\nu_D}{1 + \nu_R/\nu_D})$$

APPENDIX B

The data measured from I-V

(a) Sample #1: Al(1%Si)/$\mathrm{Ti}_{03}\mathrm{W}_{07}$/n-Si/Al(1%Si)

Index	Curve#	votage	current
1	1	0 V	267.53nA
2	1	5 mV	640.48nA
3	1	10 mV	1.1294μA
4	1	15 mV	1.7187μA
5	1	20 mV	2.4375μA
6	1	25 mV	3.2807μA
7	1	30 mV	4.3094μA
8	1	35 mV	5.5546μA
9	1	40 mV	7.0496μA
10	1	45 mV	8.8325μA
11	1	50 mV	11.013μA
12	1	55 mV	13.62 μA
13	1	60 mV	16.784μA
14	1	65 mV	20.504μA
15	1	70 mV	25.02 μA
16	1	75 mV	30.456μA
17	1	80 mV	36.912μA
18	1	85 mV	44.49 μA
19	1	90 mV	53.573μA
20	1	95 mV	64.381μA
21	1	100 mV	77.078μA
22	1	105 mV	91.81 μA
23	1	110 mV	110.39μA
24	1	115 mV	131.38μA
25	1	120 mV	155.51μA
26	1	125 mV	183.69μA
27	1	130 mV	216.42μA
28	1	135 mV	253.87μA
29	1	140 mV	296.02μA
30	1	145 mV	344.46μA

(a) Continue

Index	Curve#	vd	id
31	1	150 mV	399.14μA
32	1	155 mV	460.25μA
33	1	160 mV	527.21μA
34	1	165 mV	602.18μA
35	1	170 mV	684.44μA
36	1	175 mV	774.1 μA
37	1	180 mV	869.67μA
38	1	185 mV	973.92μA
39	1	190 mV	1.087 mA
40	1	195 mV	1.2059mA
41	1	200 mV	1.3296mA
42	1	205 mV	1.462 mA
43	1	210 mV	1.6004mA
44	1	215 mV	1.7447mA
45	1	220 mV	1.8928mA
46	1	225 mV	2.0481mA
47	1	230 mV	2.2086mA
48	1	235 mV	2.3738mA
49	1	240 mV	2.5411mA
50	1	245 mV	2.7151mA
51	1	250 mV	2.8932mA
52	1	255 mV	3.0726mA
53	1	260 mV	3.258 mA
54	1	265 mV	3.4467mA
55	1	270 mV	3.6387mA
56	1	275 mV	3.8315mA
57	1	280 mV	4.0292mA
58	1	285 mV	4.2296mA
59	1	290 mV	4.4328mA
60	1	295 mV	4.5013mA

(b) Sample #2: $\mathrm{Ti}_{03}\mathrm{W}_{07}$/n-Si/Al(1%Si)

Index	Curve#	vd	id
1	1	0 V	253.09nA
2	1	10 mV	6.7799μA
3	1	20 mV	16.096μA
4	1	30 mV	28.689μA
5	1	40 mV	46.351μA
6	1	50 mV	69.702μA
7	1	60 mV	103.52μA
8	1	70 mV	146.23μA
9	1	80 mV	202.09μA
10	1	90 mV	271.1 μA
11	1	100 mV	356.46μA
12	1	110 mV	457.17μA
13	1	120 mV	573.52μA
14	1	130 mV	707.11μA
15	1	140 mV	853.72μA
16	1	150 mV	1.02 mA
17	1	160 mV	1.1933mA
18	1	170 mV	1.3794mA
19	1	180 mV	1.5734mA
20	1	190 mV	1.7778mA
21	1	200 mV	1.9888mA
22	1	210 mV	2.2077mA
23	1	220 mV	2.4321mA
24	1	230 mV	2.6627mA
25	1	240 mV	2.8964mA
26	1	250 mV	3.1372mA
27	1	260 mV	3.3785mA
28	1	270 mV	3.626 mA
29	1	280 mV	3.876 mA
30	1	290 mV	4.1286mA

APPENDIX C

In order to illustrate the procedure of numerical calculations (Fig. 5), the summary about expression (38) is as following. Let $a = (V_a - IR) / 2V_t$ and $b = 2a$. Expression (38) can be written as: (x and y must be equal to zero)

$$y = I_{rso} [\exp (a) - \exp (- a)] + I_{so} [\exp (b) - 1] - I \qquad \text{(s - 1)}$$

and Crowell and Sze's model can be written as:

$$x = I_{so} [\exp (b) - 1] - I \qquad \text{(s - 2)}$$

where I_{rso} and I_{so} can be expressed respectively as,

$$I_{rso} = I_{r0} [1 + \frac{v_R / v_D}{1 + v_R / v_D}] \qquad \text{(s - 3)}$$

$$I_{so} = \frac{q v_R N_C S}{1 + v_R / v_D} \exp[-\frac{\phi_{Bn}}{V_t}] \qquad \text{(s - 4)}$$

Recombination term can be written as:

$$I_{recom} = I_{rso} \exp (a) [1 - \exp (- b)] \qquad \text{(s - 5)}$$

where $I_{r0} = q N_i W S / 2 \tau_r$.

REFERENCES

1. Grove, A. S. 1969. Physics and technology of semiconductor devices. Wiley, New York.

2. Yu, A. Y. C. and E. H. Snow. 1968. Surface effects on metal-silicon contacts. J. Appl. Phys. Vol. 39, pp 3008.

3. Gossick, B. R. 1963. metal-semiconductor rectifiers and transistor. Solid-St. Electron. Vol. 6, pp 445-452.

4. Crowell C. R. and M. Beguwala, 1971. Recombination velocity effects on current diffusion and imref in Schottky barriers. Solid-State Electron. Vol. 14, pp 1149-1157.

5. Crowell, C. R. and S. M. Sze, 1966. Current transport in metal-semiconductor barriers. Solid-St. Electron. Vol. 9, pp 1035-1048.

6. Scharfetter, D. L. 1965. Minority carrier injection and charge storage in epitaxial Schottky barrier diodes. Solid-St. Electron. Vol. 8, pp 299-311.

7. Rhiderick, E. H. 1978. Metal-semiconductor contacts. Clarendon Press, Oxford.

8. Padovani, F. A. and R. Stratton, 1966. Field and thermionic-field emission in Schottky barriers. Solid-St. Electron. Vol. 9, pp 695-707.

9. Henisch, H. K. 1957. Rectifying semiconductor contacts. Clarendon Press, Oxford.

10. Cunningham, J. A., C. R. Fuller and C T. Hauwood. 1970. Corrosion resistance of several integrated-circuit metallization systems. IEEE Trans. Reliab. Vol. 19, p182.

11. Harris, J. M., S. S. Lau and M. A. Nicolet. 1976. Studies of the Ti-W metallization system on Si. J. Electrochem. Soc. Vol. 123, p 120.

12. MacDonald, J. R. 1962. Accurate solution of an idealized one-carrier metal-semiconductor junction problem. Solid-State, Electron. Vol. 5, pp 11-37.

13. Racko, J., D. Donoval, M. Barus. 1992. Revised theory of current transport through the Schottky structure Solid-State, Electron. Vol. 35, pp 913-919.

14. Shenai, K. 1985. Modeling and characterization of dopant redistribution in metal and silicide contacts. IEEE Trans. Electron Devices. ED-32, p 793.

15. Hartsough, L. D. 1979. Resistivity of bias-sputtered Ti-W films. Thin Solid Films. Vol. 64, pp 17-23.

16. Hansen, M. and A. Anderko. 1958. Constitution of Binary Alloys. McGraw-Hill, New York.

17. Hill, M. 1980. Magnetran sputtered Titanium-Tungsten films. Solid State Technology, Vol. 23 (1), p 53.

18. Totta, P. A. and R. P. Sopher. 1969. SLT device metallurgy and its monolithic extension. IBM J. Res. Dev. Vol. 13, p 226.

19. Ghate, P. B., J. C. Blair, C. R. Fuller and G. E. McGuire. 1978. Application of Ti:W barrier metallization for integrated circuits. Thin Solid Films. Vol. 53, pp 117-128.

20. Wolters, R. A. M. and A. J. M. Nellissen. 1986. Properties of reactive sputtered TiW. Solid State Technol. Vol. 29, pp 131-136.

21. Nowicki, R. S., J. M. Hreeis, M. A. Nicolet and I. V. Mitchell. 1978. Studies of the Ti-W/Au metallization on aluminum. Thin Solid Films, Vol. 53, pp 195-205.

22. Stratton, R. 1962. Diffusion of hot and cold electrons in semiconductor barriers. Phys. Rev. Vol. 126, p 2002.

23. Babcock, S. E. and K. N. Tu. 1986. Titanium-tungsten contacts to silicon. Stability against aluminum penetration. J Appl. Phys. Vol. 59 (5), pp 1599-1605.

24. Babcock, S. E. and K. N. Tu. 1982. Titanium-tungsten contacts to Si: the effects of alloying on Schottky contact and on silicide formation. J Appl. Phys. Vol. 53 (10), pp 6898-6905.

25. Sze, S. M. 1982. Physics of semiconductor devices. Wiley, New York.

26. Sze, S. M. 1969. Physics of semiconductor devices. Cha. 2 and 8. Wiley, New York.

27. Ting C. Y. and M. Wittmer. 1982. The use of Titanium based contact barrier layers in Silicon technology. Thin Solid Films. Vol. 96, pp 327-345.

28. Rideout, V. L. and C. R. Ceowell. 1970. Effects of image force and tunneling on current transport in metal-semiconductor (Schottky barrier) contacts. Solid-State Electron. Vol. 13, pp 997-1009.

29. Shockley, W. and W. T. Read. 1952. Statistics of the recombination of holes and electrons. Phys. Rev. Vol. 87, p 835.

30. Hall, R. N. 1952. Electron-hole recombination in Germanium. Phys. Rev. Vol. 87, p.387.

31. Norde, H. 1979. A modified forward I-V plot for Schottky diodes with high series resistance. J. Appl. Phys. Vol. 50(7), pp 5052-5053.

32. Mclesn, A. B. 1986. Limitations to the Norde I-V plot. Semicondu. Sci. Technol. Vol. 1, pp 177-179.

33. Kousik, G. S., Z. G. Ling, and P. K. Ajmera. 1992. Nondestructive technique to measure bulk lifetime and surface recombination velocities at the two surfaces by infrared absorption due to pulsed optical excitation. J. Appl. Phy. Vol. 72, p141.

34. Schacham, S. E. and E. Finkman. 1992. Saturation current and excess carrier distribution in exponentially graded p-n junctions. J. Appl. Phy. Vol. 71, p 4997.

35. Sasaki, A. and N. Peter Robson. 1991. Carrier transport processes in p-n junction layers with a distribution of trap levels. Solid-State Electron. Vol. 34, pp 959-967.

36. Yisong, Dai and Chen Hesin. 1991. Current noise due to generation and recombination of carriers in forward-biased p-n junctions. Solid-State Elec. Vol. 34, pp 259-264.

37. Furlan, R., Van Der Spiegel, J. W. Swart. 1991. Study of the thermal stability of the Al/TiW/TiSi/Si structure. J. Elec. Soci. Vol. 138, pp 2377-2381.

38. Wolf, S. and R. N. Tauber. 1990. Silicon processing for the VLSI era. Vol. 1, Process technology. Lattice Press, Sunset beach, CA.

39. Wolf, S. and R. N. Tauber. 1990. Silicon processing for the VLSI era. Vol. 2, Process integration. Lattice Press, Sunset beach, CA.

40. Andrews, J. M. 1974. The role of the metal-semiconductor interface in silicon integrated circuit technology. J. Vac. Sci. Technol. Vol. 11, pp 972-983.

41. Bardeen, J. 1947. Surface state and rectification at a metal-semiconductor contact. Phys. Rev. Vol. 71, pp 717-727.